Programming pH-Triggered Self-Assembly via Isomerization of Peptide Sequence

Honors Thesis

Presented in partial fulfillment of the requirements for graduation

with honors research distinction in Biochemistry in the

undergraduate colleges of The Ohio State University

By

Eric Dobson

The Ohio State University

2014

Honors Committee:

Professor Joshua Goldberger, Advisor

Professor Jane Jackman

Professor Harald Vaessin

Abstract

The creation of dynamic materials that undergo morphological transitions with respect to environmental factors may aid in the targeting and treatment of various diseases. A hallmark of cancer is the presence of low extracellular pH within tumors. Therefore, the creation of novel diagnostic agents that undergo morphological transitions at precise pH values in the bloodstream can allow for the enhanced accumulation of imaging agents in tumor tissue due to differences in diffusion properties of different assembled states. Peptide amphiphiles (PAs) are an intriguing class of biocompatible vehicles that are comprised of a lipid tail, a short sequence of amino acids, and may be functionalized with various therapeutic or diagnostic moieties. PAs have been observed to undergo a micelle-to-nanofiber (basic-to-acidic) transition at a broad range of pH values in simulated serum environments. This transition is known to be tunable via alterations in the identity of the amino acid residues, the number of charged residues, the ionic strength of the solution, and the length of the fatty acid tail. However, until now no study has investigated the effects of rearranging the position of amino acid residues on self-assembly behavior. Here, using palmitoyl-IAAAEEEE-NH_2 and palmitoyl-IAAAEEEEK(DO3A:Gd)-NH_2 as well-characterized control PA systems, I studied how sequence variation controls the self-assembly behavior, specifically in the novel systems of palmitoyl-AIAAEEEE-NH_2 and palmitoyl-AIAAEEEEK(DO3A:Gd)-NH_2. Interestingly, moving the hydrophobic isoleucine one amino acid away from the palmitoyl tail increases the pH of transition between spherical micelles and nanofibers by

greater than 2 pH units. By increasing the distance between the isoleucine and the alkyl tail, the tendency of the side chain to collapse hydrophobically with the alkyl tail is reduced, allowing increased participation in hydrogen bonding beta-sheets and stabilizing the nanofiber. These findings reveal a novel strategy for programming pH-triggered self-assembly by isomerizing the peptide sequence.

Acknowledgments

The time and effort I put into this project would not have been possible without the financial support of a 2013 Pelotonia Undergraduate Fellowship. Therefore, I would like to thank Jeffrey Mason and all of the Pelotonia riders who helped raise money for this and other scholarships. I would also like to thank my advisor, Dr. Josh Goldberger, and the entire Goldberger group for the countless ways they have supported me over the past three years or so. I would also like to extend a special thanks to Arijit Ghosh who was of particular help in this project. Finally, thanks to all my friends and family for their support throughout these past three years.

Vita

August 17, 1991…….....	Born—Cincinnati, Ohio
2010…….....	Lakota West High School, Ohio
2014.....	B.S. Biochemistry, The Ohio State University, Ohio

Fields of Study

Major Field: Biochemistry

Table of Contents

List of Figures

List of Abbreviations

CD- Circular dichroism
CG- Coarse-grained
DCM- Dichloromethane
DIPEA- *N*,*N*-Diisopropylethylamine
DMF- *N,N*-Dimethylformamide
DO3A-1,4,7,10-tetraazacyclododecane-1,4,7,10-tetraacetic acid
DOTA- 1,4,7,10-tetraazacyclododecane-1,4,7-triacetic acid tri t-butyl ester
EPR- Enhanced permeability and retention effect
ESI-MS- Electrospray ionization mass spectrometry
FMOC- Fluorenylmethyloxycarbonyl chloride
HBTU- *O*-(Benzotriazol-1-yl)-*N,N,N′,N′*-tetramethyluroniumhexafluorophosphate
HATU- *O*-(7-Azabenzotriazol-1-yl)-*N,N,N′,N′*-tetramethyluroniumhexafluorophosphate
HOAt- 1-Hydroxy-7-azabenzotriazole
HOBt-1-Hydroxybenzotriazole hydrate
HPLC- High performance liquid chromatography
MD- Molecular dynamics
MRI- Magnetic Resonance Imaging
Mtt- Methyl trityl
PA- Peptide amphiphile
PTFE- Polytetrafluoroethylene
TEM- Transmission electron microscopy
TFA- Trifluoracetic acid
TIS- Triisopropylsilane
TLC- Thin layer chromatography
TOF- Time of flight

Chapter 1

Introduction

Cancer is a leading cause of death worldwide. According to the World Health Organization, cancer caused 7.6 million deaths in 2008 (approximately 13% of worldwide deaths)[1]. An increase in early detection rates for all cancer types is paramount for increasing survival rates. For example, the 5-year survival rate for breast cancer diagnosed at a localized stage is 98.6%, while the 5-year survival rate once the cancer has metastasized is only 23.3%[2]. For these reasons, the demand for imaging agents capable of selectively targeting tumor tissue at earlier stages is rising.

Since the late 1990s, the growing field of molecular biology and the increasing ease with which genomes can be sequenced have promoted the usage of personalized medicine, or the customization of treatment based on a patient's genetic information. With regards to cancer, the sequencing of the genome of cancerous cells in comparison to healthy cells has led to treatment options involving matching specific active tumor-targeting drugs to patients whose tumors match the specified genome[3]. Although this approach often leads to initial improvements in a patient's condition, these gains are many times followed by the aggressive reappearance of tumor growth and eventual death of the patient[4]. This mysterious and devastating phenomenon was recently elucidated by a study finding genetic deviations not only between cancerous cells and healthy cells, but

also among cells within a single tumor[5]. Tumor heterogeneity is the downfall of personalized medicine because, while the targeted cancerous cells may be killed off, any cancer cells present without the targeted surface markers return (and in greater numbers). The research outlined in this thesis is part of a larger plan to pursue a strategy for tumor imaging which relies on the characteristics that are alike in all forms of cancer. This model may be useful for targeted drug delivery applications in the future.

Recent research has indicated that size and shape of intravenously injected nanomaterials significantly affect biodistribution[6,7,8,9]. This phenomenon has been in part explained by the enhanced permeability and retention (EPR) effect in which nanoparticles of low zeta-potential, high solubility, and of between 20 and 200 nm diameter tend to evade immune system recognition and organ clearance leading to longer circulation lifetimes[10]. With regards to shape, cylindrical polymeric fibers have been shown to have a 10 times longer circulation time in the bloodstream than their spherical counterparts[11]. When targeting cancer, the high interstitial fluid pressure of tumor tissue results in diffusion becoming the most important mass transport process. Therefore, vehicles of small diameter permeate tumor tissue most easily. Therapeutic attempts at exploiting this effect have been ineffective due to small vehicles both entering and leaving tumor tissue at enhanced rates, leading to decreased accumulation[12]. Therefore, a vehicle that begins with a small diameter to permeate the tumor tissue and transforms into a vehicle of larger diameter to enhance retention within the tumor would be ideal. However, most nanomaterials previously investigated are either static objects which do

not transform in the cancer environment or fragment into smaller pieces to release an imaging or medicinal load upon reaching their target[13].

Designing nanomaterials that spontaneously change shape and size in response to physiological stimuli allows for the exploitation of the aforementioned different diffusion kinetics of nanosized carriers, enhancing their accumulation at a given target. Although cancer refers to not one, but many diseases, most forms of cancers possess at least two exploitable characteristics. The first of these is a slightly acidic microenvironment (pH 6.6-7.4)[14] resulting from the enhanced rate of glycolysis in the rapidly growing cancer cells. The second, also resulting from uncontrolled growth and relating most directly to diffusion kinetics, is the leaky and irregular lymphatic vasculature resulting in an enhanced permeability and retention of nano-sized particles.

To take advantage of these two features, this thesis makes use of a class of molecules known as peptide amphiphiles (PAs)[15]. PAs are an attractive class of molecules for the purpose of targeting cancer cells for several reason: they can spontaneously self-assemble into nanofibers, their intermolecular forces may be tuned precisely via modification to their peptide sequence, and they are biocompatible. A goal of this thesis is to create and test a peptide amphiphile (PA) that undergoes a spherical micelle to nanofiber transition in environments similar in ionic strength and pH conditions to that of tumor tissue (Figure 1.1).

The Goldberger group has previously developed a general PA design scheme that allows for fine-tuning the transition from spherical micelles to polymeric cylindrical micelles by tenths of pH units. This design involves four main segments: a hydrophobic

alkyl tail, followed by a β sheet-forming peptide region, a charged amino acid sequence, and a C-terminal macrocyclic Gd^{3+} chelate for MRI-imaging applications (Figure 1.2). Increasing and decreasing pH is known to increase and decrease the degree of ionization of the charged sequence. This change in ionization has been found to provide a sufficient trigger for dynamic self-assembly. Exploration of this design strategy has culminated in the synthesis and characterization of a PA, palmitoyl-IAAAEEEEK(DO3A:Gd)-NH_2 (Figure 1.2), which has been observed to undergo a sphere-to-nanofiber transition at acidic pHs in simulated serum salt solution (150 mM NaCl and 2.2 mM $CaCl_2$) with a low concentration dependence (Figure 1.5). The supramolecular structure of the PA in salt solution was monitored via circular dichroism (CD) spectroscopy, critical aggregation concentration (CAC) measurements, and verified at higher concentrations using transmission electron microscopy (TEM). This transition was determined to be rapid and reversible, occurring in less than three minutes. Despite this success, the transition of palmitoyl-IAAAEEEEK(DO3A:Gd)-NH_2 from spherical micelle to nanofiber was found to occur at 5.7-6.0 pH at or above the detectable concentration limit for MRI applications (10 μM)[16]. This transition pH is significantly lower than the 6.6-7.4 pH range necessary for tumor targeting applications. The parent molecule of this MRI-active derivative has also been synthesized and studied: palmitoyl-IAAAEEEE-NH_2 (Figure 1.3). Under identical conditions, this PA exhibited a sphere-to-cylinder transition with significantly higher concentration dependence (Figure 1.4)[17]. Therefore, further optimization is required to develop a PA capable of pH-triggered tumor targeting.

Previous studies involving peptides and peptide amphiphiles have explored the relationship between sequence variation through the rearrangement of amino acids in the peptide's primary structure and self-assembly morphology[18,19]. However, the effects of sequence isomerization have never been studied in a dynamically self-assembling system with an environmental trigger (such as pH). The purpose of this study is to establish a relationship between the position of the β sheet-forming residue in the primary peptide sequence and the pH of transition. To accomplish this, previously studied PAs were isomerized to create palmitoyl-AIAAEEEE-NH_2 (Figure 1.6) and palmitoyl-AIAAEEEEK(DO3A:Gd)-NH_2 (Figure 1.7).

In Chapter 2, the synthesis, purification, and characterization procedures for both molecules are outlined. Additionally, proof of product identity and purity is contained in Chapter 2. Chapter 3 describes the construction of pH- and concentration-dependent phase diagrams for both new PAs. This process includes data collected via CD, CAC measurements, and images taken using conventional TEM. Chapter 4 extensively compares the phase diagrams of the newly synthesized isomers with their previously characterized parent molecules. Chapter 5 provides a summary of this thesis as well as future work planned in this area.

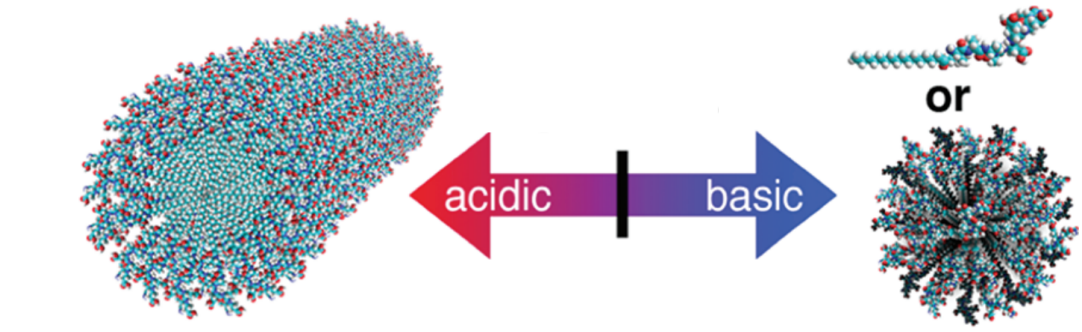

Figure 1.1: Illustration of previously observed peptide amphiphile self-assembly behavior

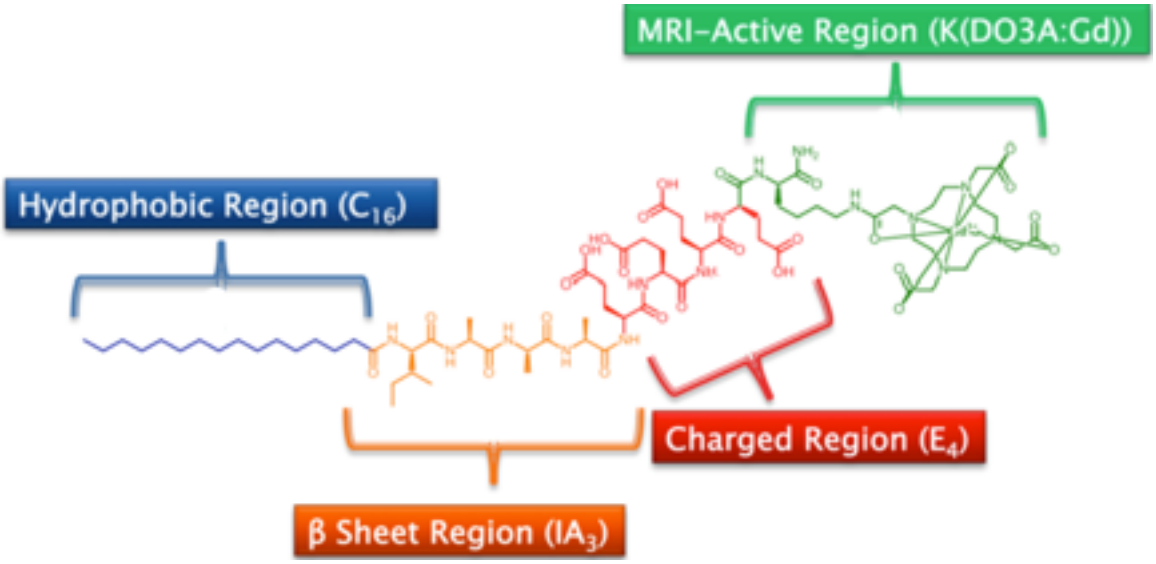

Figure 1.2: Schematic representation of a peptide amphiphile contrast agent, showing the 4 regions contributing to the molecules unique, self-assembling properties are shown; the hydrophobic region (Blue), β sheet-forming region (Orange), the charged region (Red), and the MRI-Active region (green). Note: PA shown here is palmitoyl-IAAAEEEEK(DO3A:Gd).

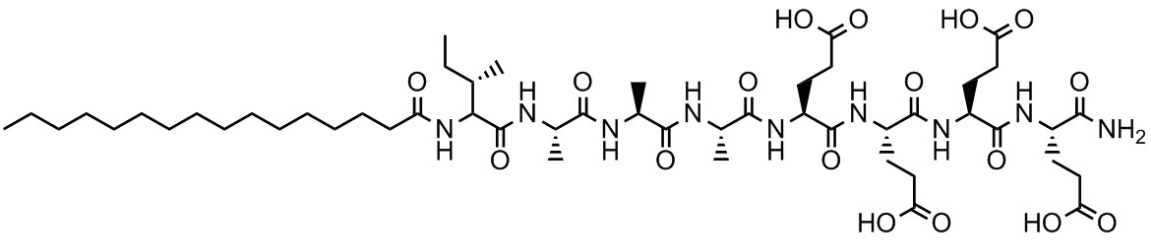

Figure 1.3: Structure of palmitoyl-IAAAEEEE-NH_2

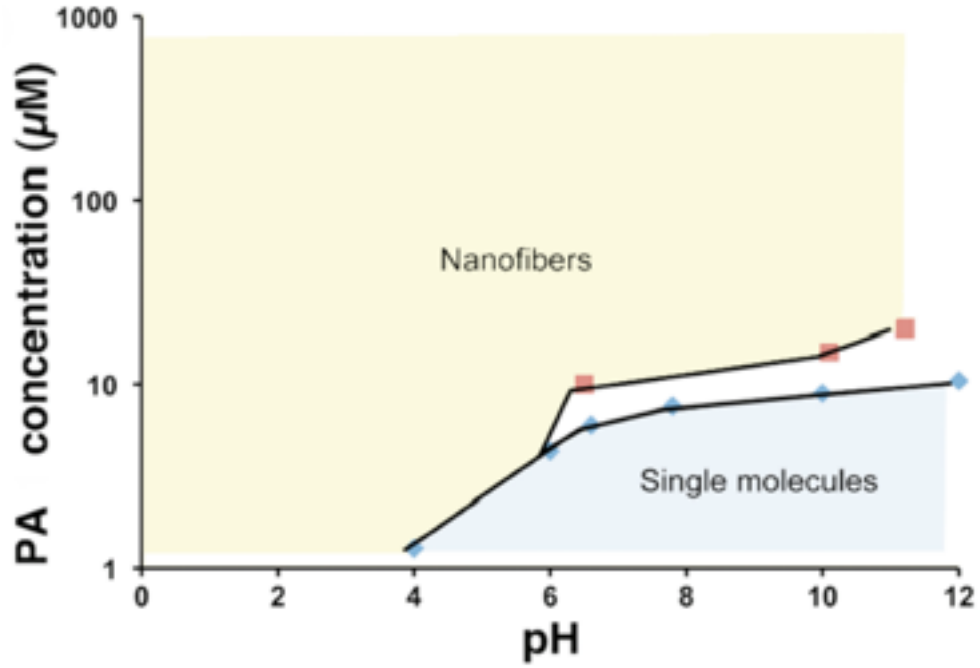

Figure 1.4: Concentration and pH dependent phase diagram for palmitoyl-IAAAEEEEK(DO3A:Gd)-NH_2 in 150 mM NaCl, 2.2 mM $CaCl_2$[17]

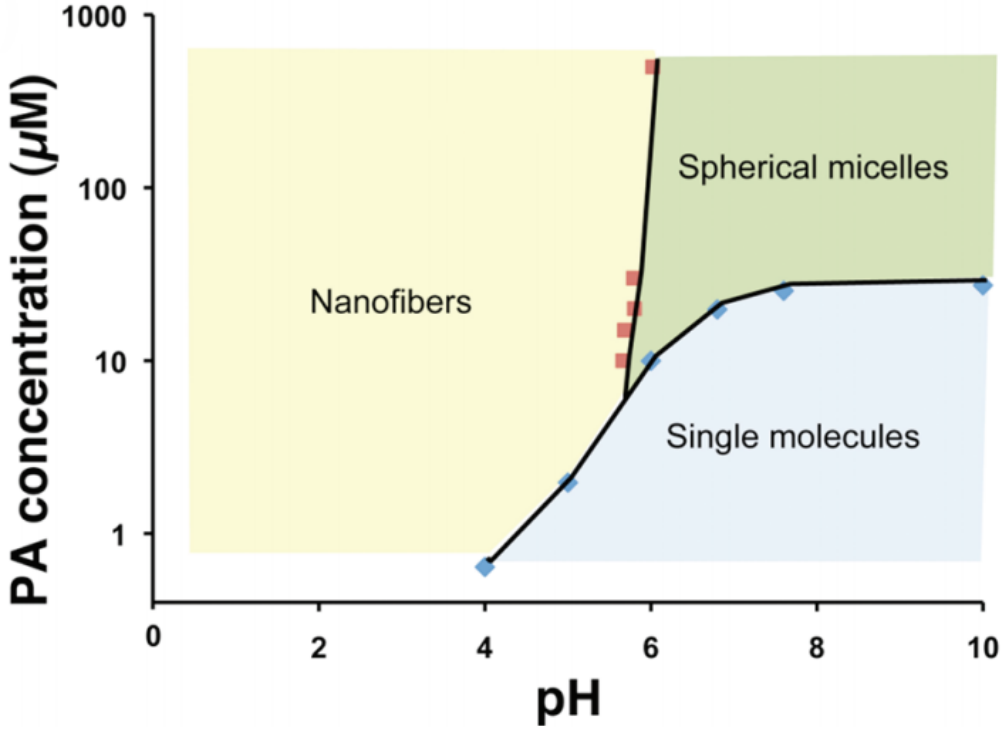

Figure 1.5: Concentration and pH dependent phase diagram for palmitoyl-IAAAEEEEK(DO3A:Gd)-NH_2 in 150 mM NaCl, 2.2 mM $CaCl_2$[17].

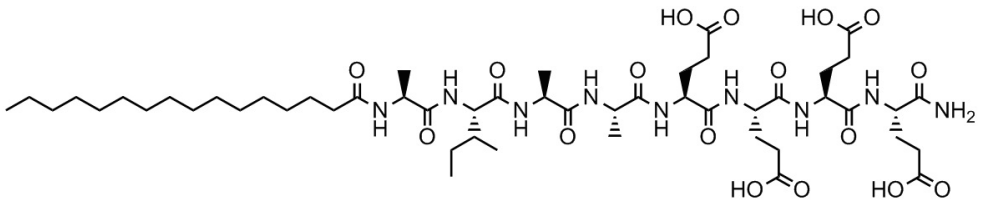

Figure 1.6: Structure of palmitoyl-AIAAEEEE-NH_2

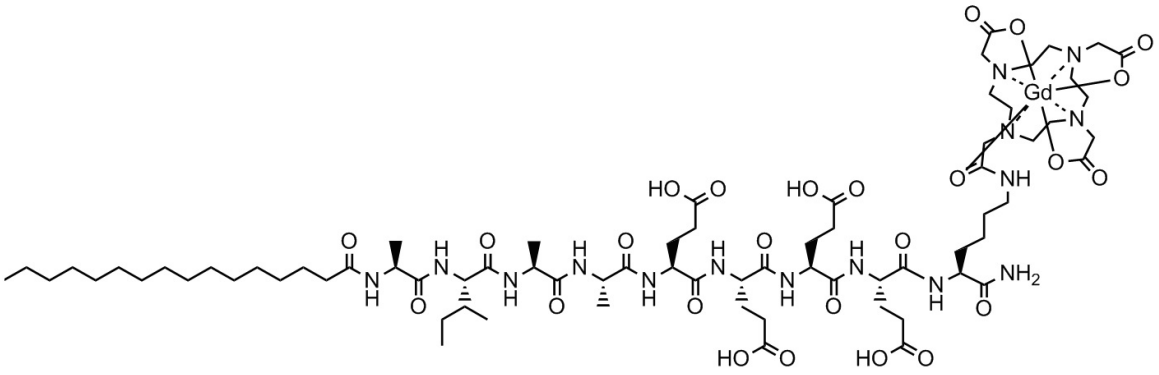

Figure 1.7: Structure of palmitoyl-AIAAEEEEK(DO3A:Gd)-NH_2

Chapter 2

Materials and Methods

Synthesis of Peptides Amphiphiles

For this study, two peptide amphiphiles were created: palmitoyl-AIAAEEEE-NH_2 and palmitoyl-AIAAEEEEK(DO3A:Gd)-NH_2. Both peptide amphiphiles were synthesized using amino acids purchased from AnaSpec Inc. unless otherwise noted. PAs were built upon a Sieber resin using standard FMOC chemistry[20] from the C-terminus to N-terminus. PAs were synthesized manually on a 0.50 mmol scale using the following procedure:

The Sieber resin was placed in a shaker vessel and swelled with dichloromethane (DCM) for 30 minutes, then again swelled with dimethyl formamide (DMF) for 30 minutes. The solvent was removed and a solution of 20% N,N-Diisopropylethylamine (DIPEA) in DMF was added to the vessel. The mixture was shaken for 10 minutes. The solution was drained, replenished, and shaken for another 10 minutes. The DIPEA/DMF solution was drained again and the resin was rinsed several times with DMF, then with DCM. A Kaiser test was used to confirm the removal of the FMOC protecting group. To couple amino acids to the deprotected resin or peptide chain, activation of the amino acid using O-Benzotriazole N,N,N',N'-tetramethyluroniumhexafluorophosphate (HBTU) or, for higher coupling efficiency, 2-(7-Aza-1H-benzotriazole-1-ly)-1,1,3,3-tetramethyluronium hexafluorophosphate (HATU) was employed. Each coupling

solution contained 3.95 equivalents of the amino acid desired, 4 equivalents of N-hydroxybenzotriazole (HOBt) or 1-Hydroxy-7-azabenotriazole (HOAt), 4 equivalents of HBTU or HATU, and 6 equivalents of DIPEA with respect to peptide. A few drops of Triton X-100 (surfactant) were also added to prevent aggregation and increase coupling efficiency. The coupling solution was dissolved in DMF, mixed, and added to the shaker vessel. Each coupling reaction was allowed at least 2 hours to shake before the next deprotection.

Cleavage from Resin

Following completion of the peptide, palmitoyl-AIA_2E_4-NH_2 was cleaved using a highly acidic trifluoroacetic acid (TFA) cocktail containing 95% TFA, 2% Millipore water, 2% anisole, and 1% triisopropylsilane. This cocktail ensured removal of peptide from the resin as well as deprotection of the *tert*-butyl ester groups from the glutamic acid residues. The cocktail was added to the resin and shaken for 3 hours, followed by a 30 minute rinse with DCM. Following cleavage, palmitoyl-AIA_2E_4-NH_2 was rotovapped to remove DCM and TFA. The peptide was then crashed out of solution using cold diethyl ether. The precipitate was filtered and purified (see section below).

Following termination of palmitoyl-AIA_2E_4K-NH_2 with a palmitic acid tail, a mildly acidic cleavage cocktail was prepared. The cleavage cocktail contained 96% DCM, 2% anisole, 1% triisopropylsilane, and 1% TFA**.** This cocktail ensured removal of the peptide from resin and the removal of the lysine residue's Mtt protecting group while

maintaining the *tert*-butyl ester protection of the glutamic acid residues.100 mL of the cleavage cocktail was prepared. The cocktail was added to the resin in 20 mL increments and allowed to shake for 20 minutes after addition, then drained into a round bottom flask. Following exhaustion of the cleavage cocktail, a final rinse of DCM was added to the resin and allowed to shake for 30 minutes, then drained into the flask. A portion of DIPEA equimolar to the total amount of TFA used was added to the flask and excess solvent was removed under vacuum. The peptide was crashed out of solution using cold water, then filtered.

Addition of DOTA to palmitoyl-AIAAEEEEK-NH_2

Following the precipitation palmitoyl-AIAAEEEEK-NH_2, a 1,4,7,10-tetraazacyclododecane-1,4,7-trisacetic acid (DO3A) chelate was added using solution phase coupling. The PA was added to pyridine and stirred until dissolved at 60 ^{o}C. The solution was then allowed to stir at room temperature. A coupling solution containing a small amount of pyridine, 2 equivalent HATU, 4.4 equivalents of DIPEA, and 2 equivalents of DO3A (relative the peptide) was prepared. This solution was added to the PA and the combination was stirred overnight. Excess pyridine was then removed under vacuum and the peptide was crashed out using cold water, then filtered. The resulting solid was then stirred in a deprotection cocktail containing 95% TFA, 2% Millipore water, 2% anisole, and 1% triisopropylsilane. The deprotection cocktail was stirred at room temperature for 24 hours. Excess TFA was removed under vacuum and the peptide

was precipitated out of solution using cold diethyl ether followed by filtration. The resulting solid was purified as described below.

Purification of PAs

The crude PA was dissolved in a 10% acetonitrile aqueous solution with a few drops of NH_4OH added to aid in solubility. Following dissolution, the PA solution was filtered using a 0.45 μm polytetrafluoroethylene (PTFE) filter. Purification was performed using a Shimadzu preparative high performance liquid chromatography (HPLC) system (dual pump system controlled by LC-MS solution software) with an Agilent PLRP-S polymer column (Model No. PL1212.3100 150 mm x 25 mm) under basic conditions. The product was eluted using a linear gradient from 10% acetonitrile to 20% acetonitrile over 22.5 minutes, followed by a linear gradient from 20% acetonitrile to 40% acetonitrile over an additional 67.5 minutes, both containing 0.1% NH_4OH (v/v). The presence of the desired product in collected fraction was confirmed using electrospray ionization time-of-flight mass spectrometer (ESI-TOF MS) (Bruker). The purity of product-containing samples was assayed usinga Shimadzu analytical HPLC system. Samples of high purity were combined. Pure fractions were relieved of acetonitrile under vacuum and freeze-dried to produce a white, fluffy powder. For MS confirmation of successful PA synthesis see Figure 2.1 and Figure 2.2 for palmitoyl-AIAAEEEE-NH_2 and palmitoyl-AIAAEEEEK(DO3A:Gd), respectively. For analytic

HPLC confirmation of PA purity, see Figure 2.3 and Figure 2.4 for palmitoyl-AIAAEEEE-NH_2 and palmitoyl-AIAAEEEEK(DO3A:Gd)-NH_2 respectively.

Chelation of PA with Gd^{3+}

A small amount (~15 mg) of the purified and fully deprotected palmitoyl-AIAAEEEEK(DO3A) was dissolved in water with 2 equivalents of $GdCl_3$ in 0.01 M HCl. The solution was raised to exactly 5.0 pH using small amounts of 0.05 M NaOH and stirred at 60 ^oC for 10 minutes. The reaction was brought back to room temperature and the pH was again adjusted to pH 5.0 since the reaction results in a lowering of pH. The reaction was returned to 60 ^oC and stirred overnight. The solution was then returned to room temperature and the pH was adjusted to 10 or greater using 0.1 M NaOH to precipitate excess Gd^{3+} in the form of $Gd(OH)_3$. The solution was then filtered using a 0.45 μm PTFE filter and the pH was adjusted to neutral using 0.1 M HCl. The solution was then dialyzed against Millipore water. The buffer water was changed 4 times over a 48 hours period. The dialyzed solution was then freeze-dried to create a fluffy white powder: pure palmitoyl-AIAAEEEEK(DO3A:Gd).

Circular Dichroism

Measurements were completed using a CD spectrometer (Jasco-815). Each spectra is the average of 3 accumulations, baseline subtracted using an aqueous solution

containing only 150 mM NaCl and 2.2 mM $CaCl_2$. PA solutions were prepared at basic pH containing 1.00 mM PA and no salts. Samples containing various concentrations of the aqueous PAs with 150 mM NaCl and 2.2 mM $CaCl_2$ were prepared and heated at 80 ^oC for 30 minutes at 9 or greater pH. After heating, samples were allowed to cool to room temperature and pH was adjusted as desired for CD measurements.

Determination of Critical Aggregation Concentration (CAC)

The pyrene 1:3 method[17] was used to determine CAC. For both palmitoyl-AIAAEEEEK(DO3A:Gd)-NH_2 and palmitoyl-AIAAEEEE-NH_2 CAC measurements were performed at pH of 5, 6, 7, 8, and 10. Samples of high peptide concentration (300-750 μM) were prepared containing 150 mM NaCl and 2.2 mM $CaCl_2$. These samples were raised to 9 or greater pH using dilute NaOH and heated at 80 ^oC for 30 minutes. Samples were allowed to cool to room temperature and pH was altered to the desired value using dilute NaOH and HCl. Solutions containing only aqueous 150 mM NaCl and 2.2 mM $CaCl_2$ and solutions containing these salts, a 1:1 solution of water and methanol, and 62 μM pyrene were also prepared. Each of these solutions was divided into five portions and adjusted to an appropriate pH (5, 6, 7, 8, 10). The PA solutions were serially diluted with the corresponding salt solutions with a total of 125 μL at each concentration. 5 μL of the pyrene containing solution as added to each dilution for a final pyrene concentration of 2.4 μM. Each dilution was probed for fluorescence with an excitation wavelength of 335 nm. Fluorescence was recorded with particular attention

paid to the 376 nm and 392 nm emission peaks. The ratio of these two peaks was plotted versus PA concentration on a log scale.

Transmission Electron Microscopy

TEM images were obtained at various concentrations and pH values, with 150 mM NaCl and 2.2 mM $CaCl_2$ in deionized water. Solutions were heated at 80 ^{o}C for 30 minutes in an oil bath and gradually cooled to room temperature. Following temperature equilibration, pH adjustment was achieved using HCl or NaOH. 5 µL of this solution was pipetted onto a Carbon Formvar grid (Electron Microscopy Sciences) and allowed to sit for 2 minutes before being wicked dry. The samples were negatively stained with 1 wt% uranyl acetate and imaged under a FEI Tecnai G2 Bio TWIN TEM system operating at 100 kV.

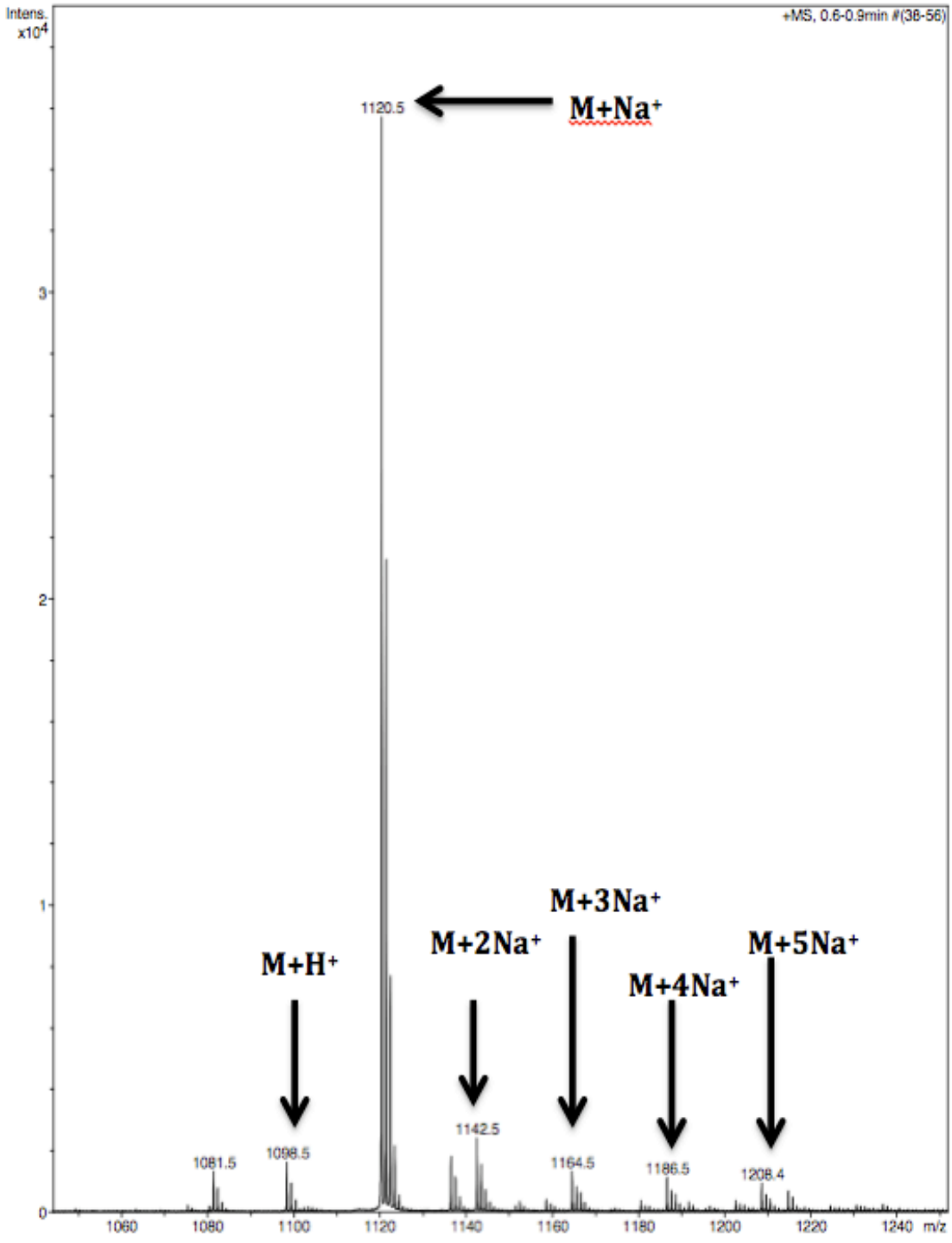

Figure 2.1: ESI-TOF mass spectrum of palmitoyl-AIAAEEEE-NH_2

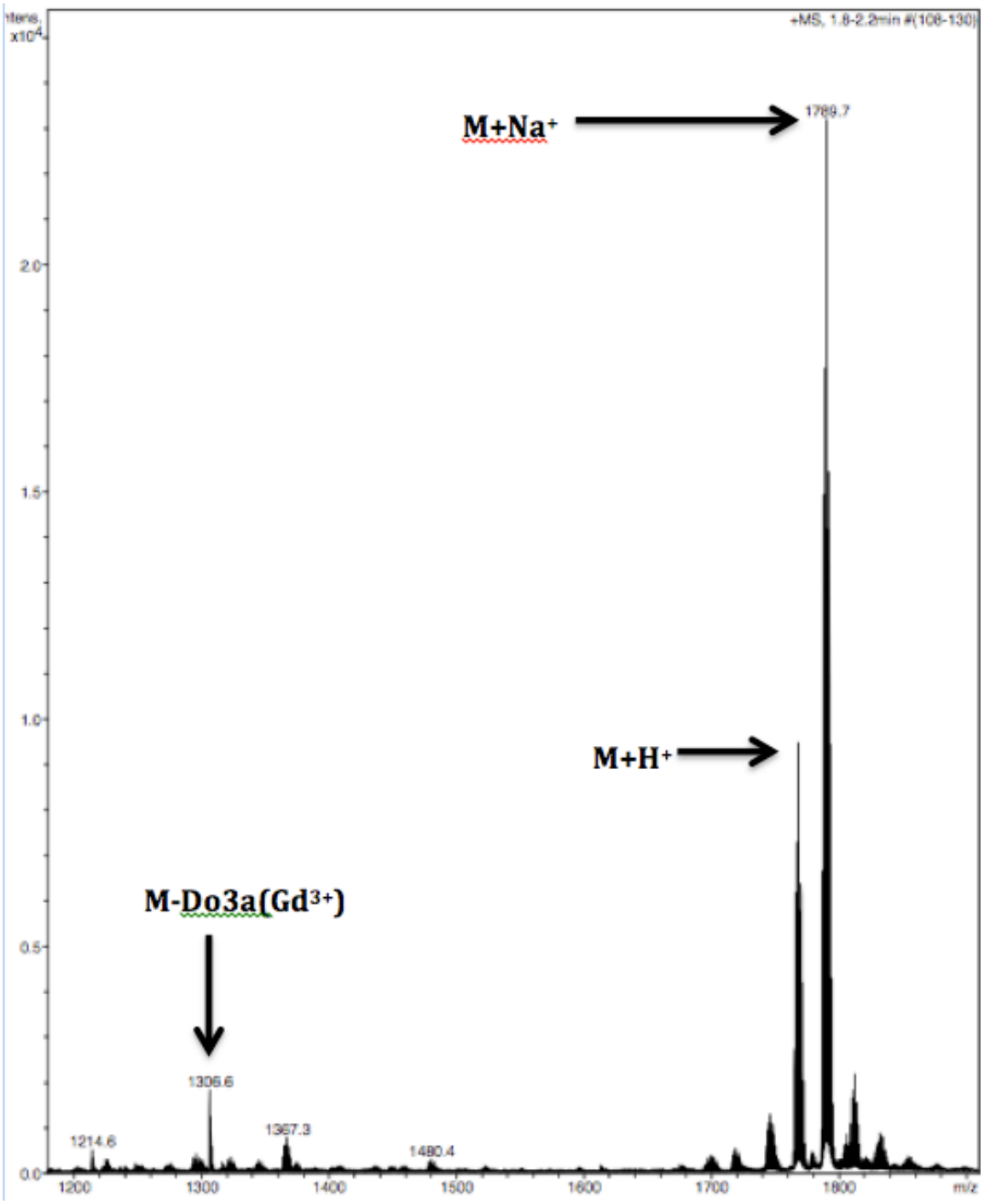

Figure 2.2: ESI-TOF mass spectrum of palmitoyl-AIAAEEEEK(DO3A:Gd)-NH_2

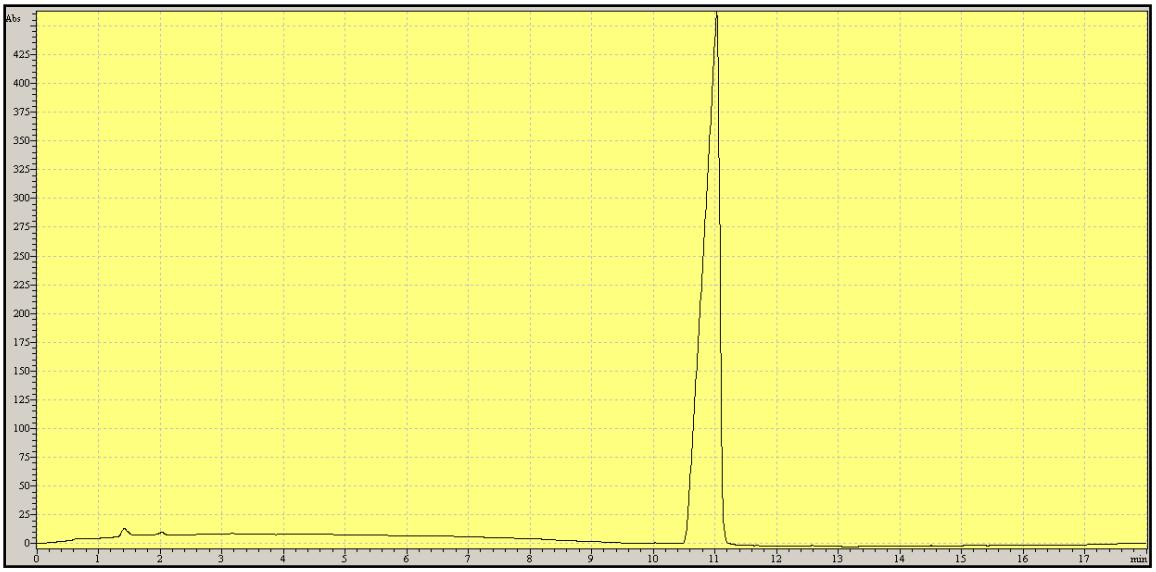

Figure 2.3: Analytic HPLC chromatogram of palmitoyl-AIAAEEEE-NH_2

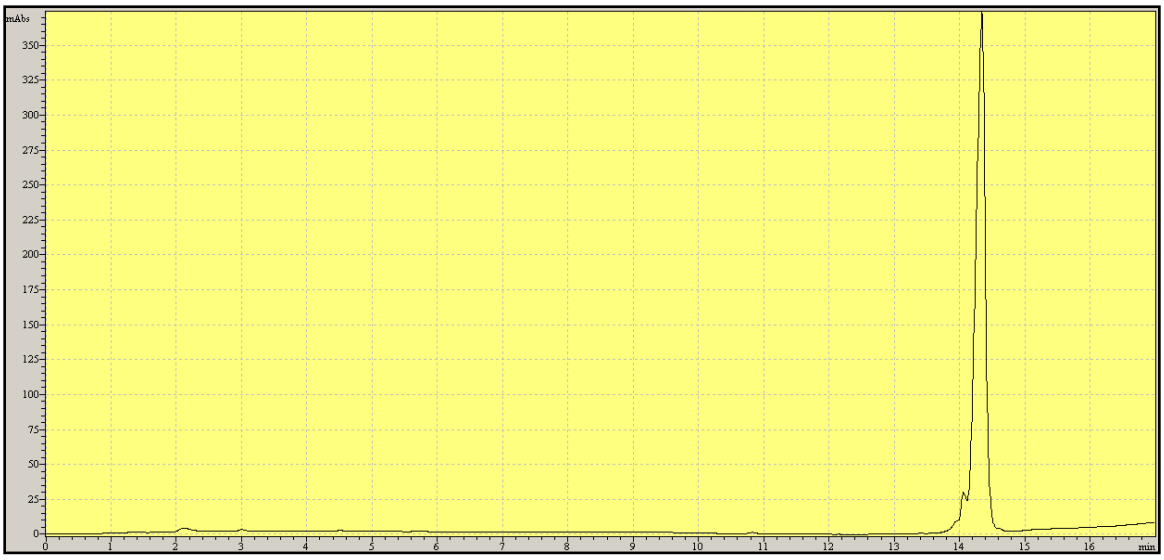

Figure 2.4: Analytic HPLC chromatogram of palmitoyl-AIAAEEEEK(DO3A:Gd)-NH_2

Chapter 3

Construction of Phase Diagrams

Following synthesis and purification, efforts were made toward creating two-dimensional (pH- and concentration-dependent) phase diagrams for both of palmitoyl-AIAAEEEEK(DO3A:Gd)-NH_2 and palmitoyl-AIAAEEEE-NH_2. All measurements for all methods, unless otherwise indicated, were performed in simulated serum salt conditions (150 mM NaCl and 2.2 mM $CaCl_2$).

Circular Dichroism

CD spectra were compiled for both palmitoyl-AIAAEEEEK(DO3A:Gd)-NH_2 and palmitoyl-AIAAEEEE-NH_2 to determine the prominent secondary structure of the peptide at concentrations of 5 μM and greater. Previously, a β sheet CD signal has been correlated to a nanofiber morphology and a random coil CD signal has been correlated to a spherical micelle or single molecule morphology[17]. When using CD, β sheet is signaled by an ellipticity minimum at 218 nm and random coil, by an ellipticity maximum at 212 nm and a minimum at 196 nm[18]. For the purpose of this simple system, the transition from spherical micelle (random coil) to nanofiber (β sheet) was determined to take place just as the ellipticity at 205 nm first became positive. This transition was observed to be concentration dependent as well, with higher concentrations favoring a β sheet secondary

structure even at high pH values. This concentration dependence was greater for palmitoyl-AIAAEEEE-NH_2 than for palmitoyl-AIAAEEEEK(DO3A:Gd)-NH_2.

CD data for palmitoyl-AIAAEEEE-NH_2 at 5 μM revealed a transition from random coil to β sheet between pH values of 7.05 and 7.12. These data are shown in their entirety in Figure 3.1. For all subsequent CD spectra, no greater than four pH-dependent traces shall be shown for the sake of clarity. Within these four shall be included the two pH-dependent traces on either side of the random coil-to-β sheet transition. At 10 μM this transition increased to pH values between 6.16 and 6.26 (Figure 3.2). At 12.5 μM the transition shifted higher still, to between pH 8.13 and 8.26 (Figure 3.3). By concentrations of 15 and 30 μM, no transition could be found and the PA exhibited a β sheet signal independent of pH (Figure 3.4 and Figure 3.5).

CD analysis of palmitoyl-AIAAEEEEK(DO3A:Gd)-NH_2 at 5 μM revealed a transition between β sheet and random coil between pH values of 6.44 and 6.55 (Figure 3.6). At 10 μM this transition point increased to between pH 7.09 and 7.15 (Figure 3.7). By 25 μM, the transition was observed between pH 7.67 and 7.80 (Figure 3.8). Between 50 μM and 150 μM, the transition seemed relatively constant, observed between pH 7.92 and 8.04 and between 7.94 and 8.05, respectively (Figure 3.9 and Figure 3.10).

The reversibility of this transition was also tested using CD. A sample of 5 μM palmitoyl-AIAAEEEEK(DO3A:Gd)-NH_2 initially was brought to pH 8.55 and a CD spectrum was acquired. This solution was then acidified to pH 5.65 and another spectrum was recorded. The solution pH was again raised back to 8.55 and spectra were recorded every 15 minutes for 45 minutes (Figure 3.11). Although the spectra reflected a random

coil signal, none of the spectra taken within the 45 minutes after returning to pH 8.55 were superimposable with the original pH 8.55 spectrum.

Critical Aggregation Concentration

The CAC for palmitoyl-AIAAEEEEK(DO3A:Gd)-NH_2 and palmitoyl-AIAAEEEE-NH_2 were determined at 5 pH values by the method described in Chapter 2. CACs for palmitoyl-AIAAEEEE-NH_2 were determined to be 2.0 μM, 2.6 μM, 2.5 μM, 3.2 μM, and 13.4 μM for pH 5, 6, 7, 8, and 10 respectively (Figures 3.12-3.15). A clear relationship between pH and CAC is evident in these data and is illustrated in Figure 3.12, which shows the CAC determination for pHs 5 and 10 superimposed in a single chart. This relationship was expected. As the PA molecule exists in a highly ionized state (at basic pH) aggregation is inhibited by ionic repulsion. When the glutamic acid residues are more protonated (at acidic pH values) this ionic repulsion is lessened or eliminated, allowing aggregation at lower concentrations.

In determining the CAC for palmitoyl-AIAAEEEEK(DO3A:Gd), a similar pH dependence was noted. The dependency is illustrated in Figure 3.16, which shows the CAC determination for pH values of 5 and 10 superimposed in a single chart. The CAC values for palmitoyl-AIAAEEEEK(DO3A:Gd)-NH_2 were determined to be 1.5 μM, 3.2 μM, 3.5 μM, 3.7 μM and 5.4 μM for pHs 5, 6, 7, 8, and 10 respectively (Figures 3.16-3.19).

Transmission Electron Microscopy and Complete Phase Diagrams

Following the collection of CD and CAC data, observed transitions were plotted with respect to pH and PA concentration to form phase diagrams for palmitoyl-AIAAEEEE-NH_2 (Figure 3.20) and palmitoyl-AIAAEEEEK(DO3A:Gd)-NH_2 (Figure 3.21). TEM images confirmed the presence of nanofibers in 100 μM and 10 μM palmitoyl-AIAAEEEE-NH_2 at pH 8.3 and pH 5.5, respectively (Figure 3.22). At 10 μM under acidic conditions these nanofibers were relatively small, generally ranging from 100-200 nm in length. At 100 μM under basic conditions, these nanofibers were significantly longer, often exceeding 1 micron in length. TEM also confirmed the presence of long nanofibers (greater than 1 micron) in 150 μM palmitoyl-AIAAEEEEK(DO3A:Gd)-NH_2 at 6.6 pH and the lack thereof at 9.9 pH (Figure 3.23). In each case that nanofibers were found, the diameter of an individual nanofiber was around 10 nm. Nanofibers were generally found in bundles with other nanofibers.

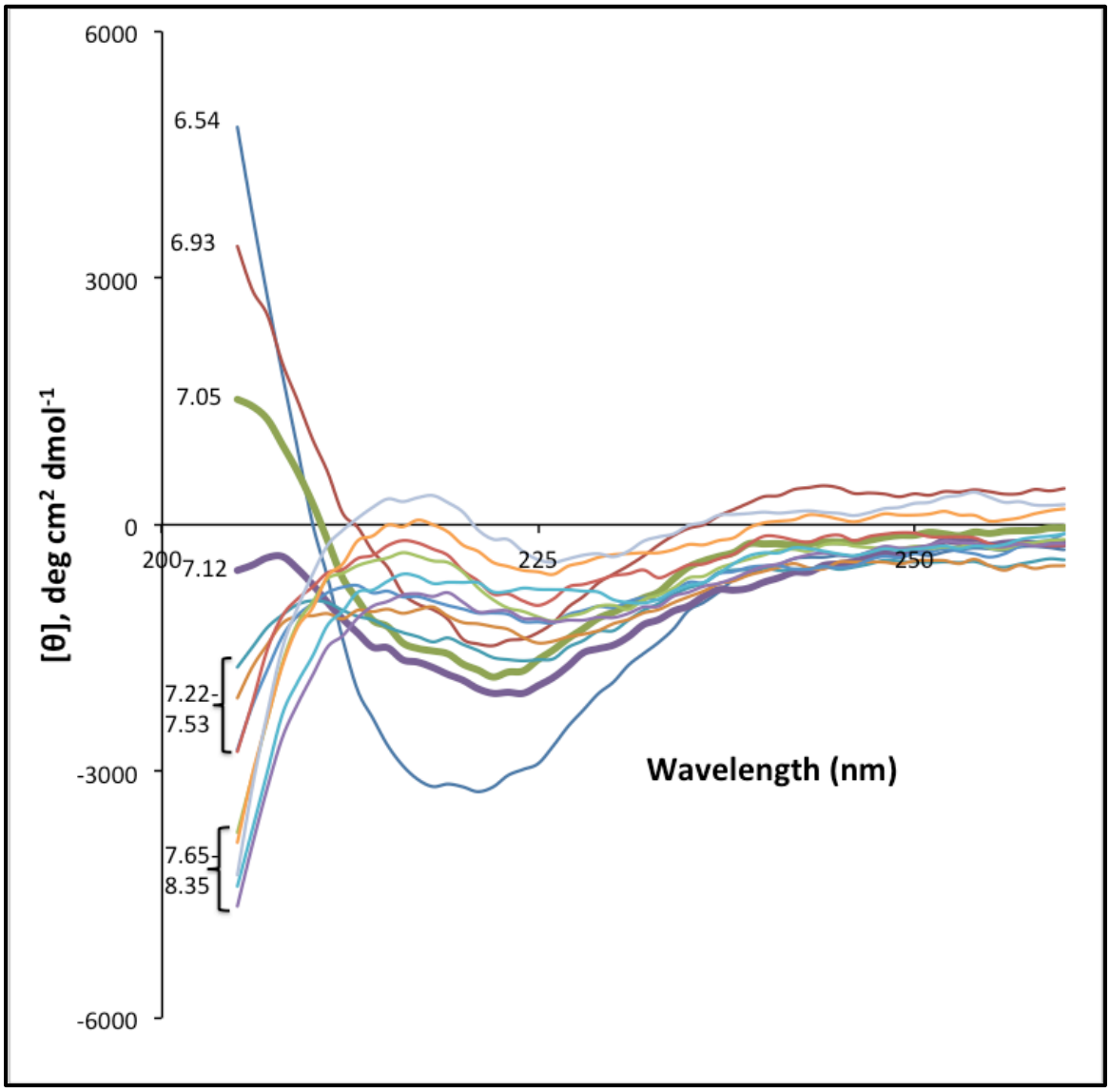

Figure 3.1: Detailed pH-dependent CD spectra of 5 μM palmitoyl-AIAAEEEE-NH_2

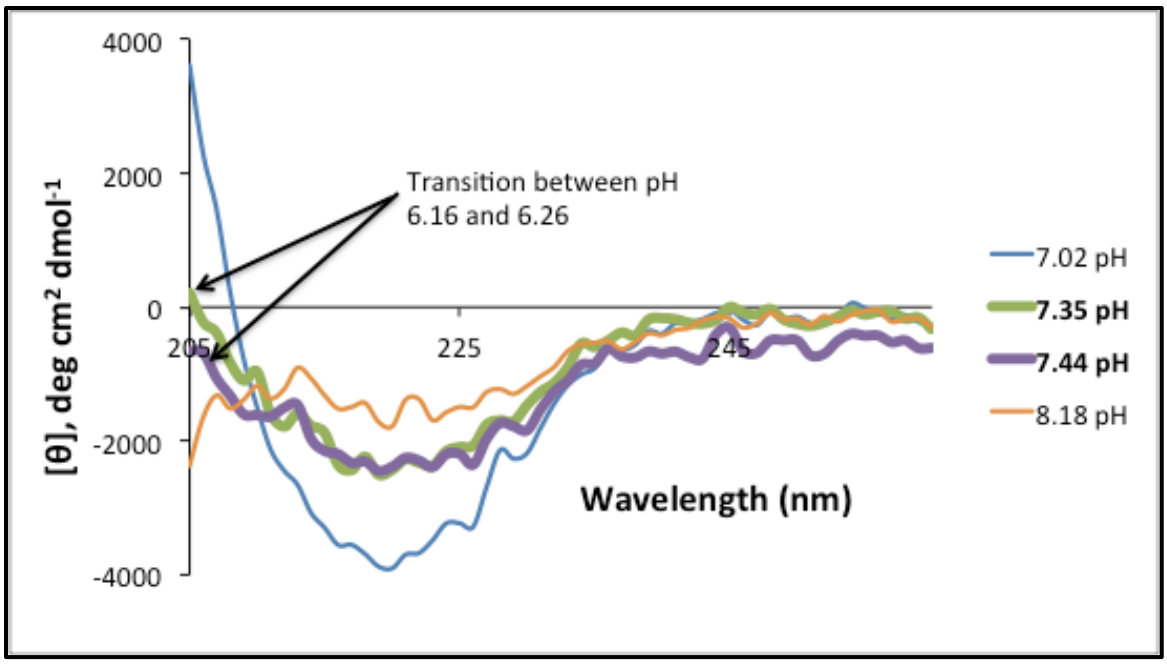

Figure 3.2: pH-dependent CD spectra of 10 µM palmitoyl-AIAAEEEE-NH_2

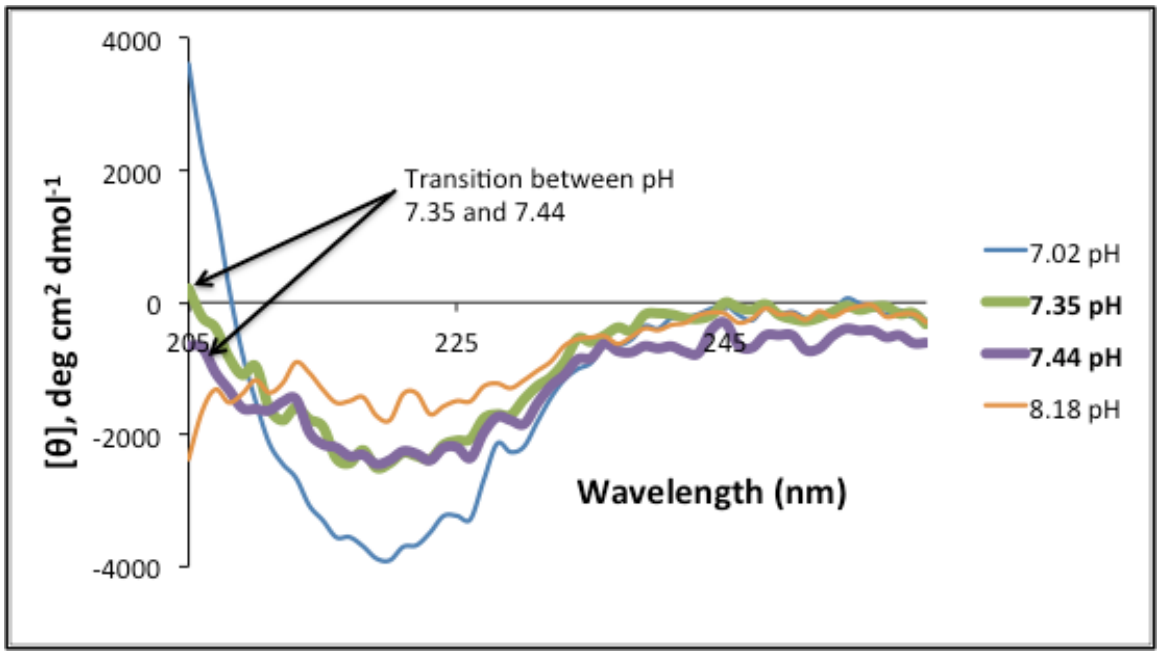

Figure 3.3: pH-dependent CD spectra of 12.5 µM palmitoyl-AIAAEEEE-NH_2

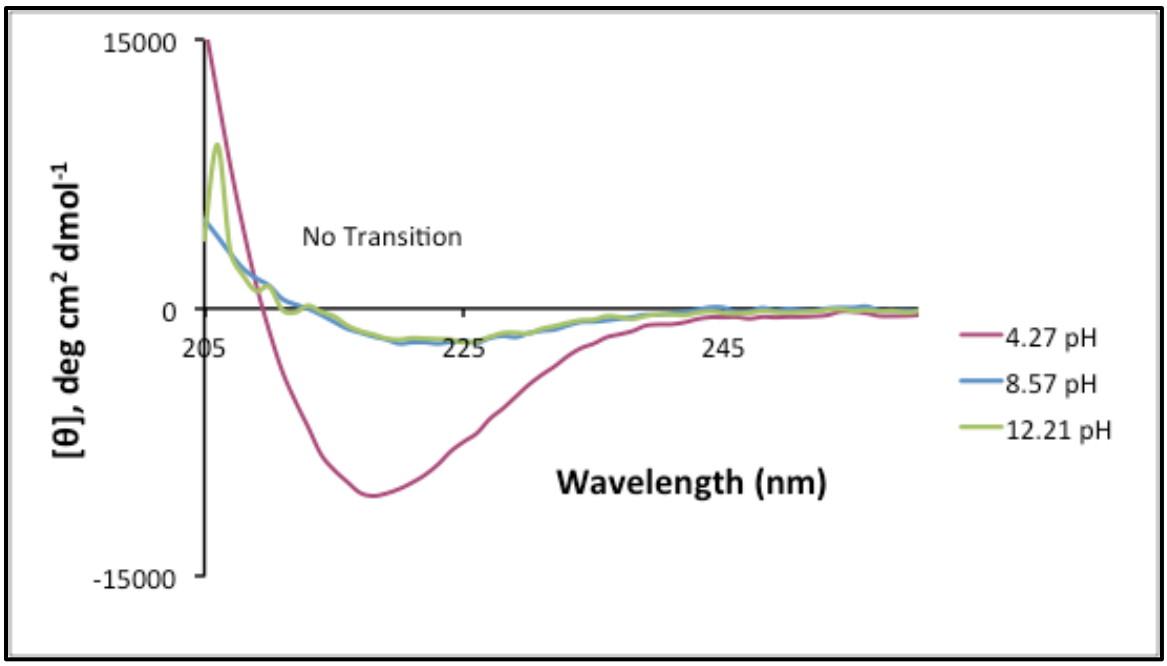

Figure 3.4: pH-dependent CD spectra of 15 μM palmitoyl-AIAAEEEE-NH_2

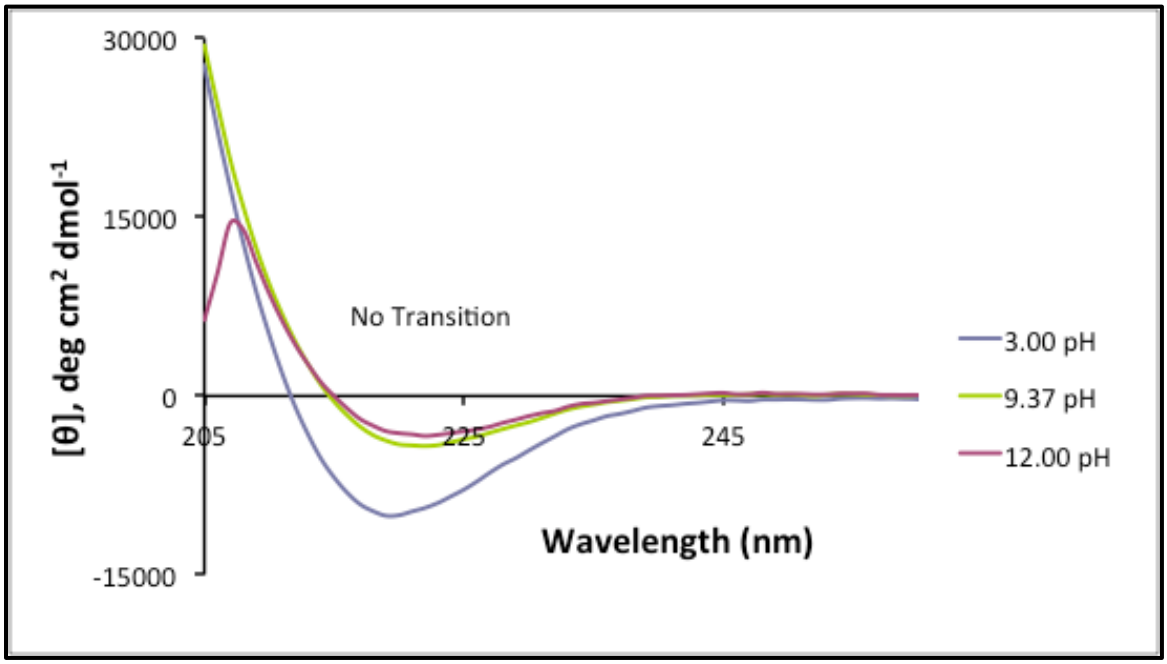

Figure 3.5: pH-dependent CD spectra of 30 μM palmitoyl-AIAAEEEE-NH_2

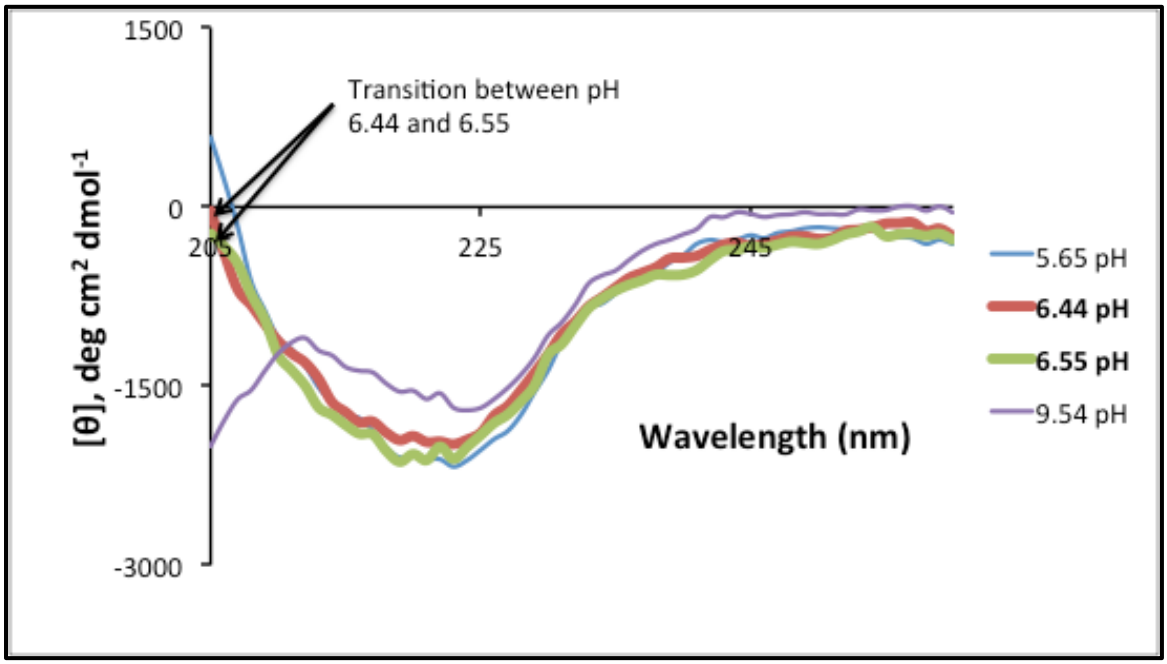

Figure 3.6: pH-dependent CD spectra of 5 µM palmitoyl-AIAAEEEEK(DO3A:Gd)-NH_2

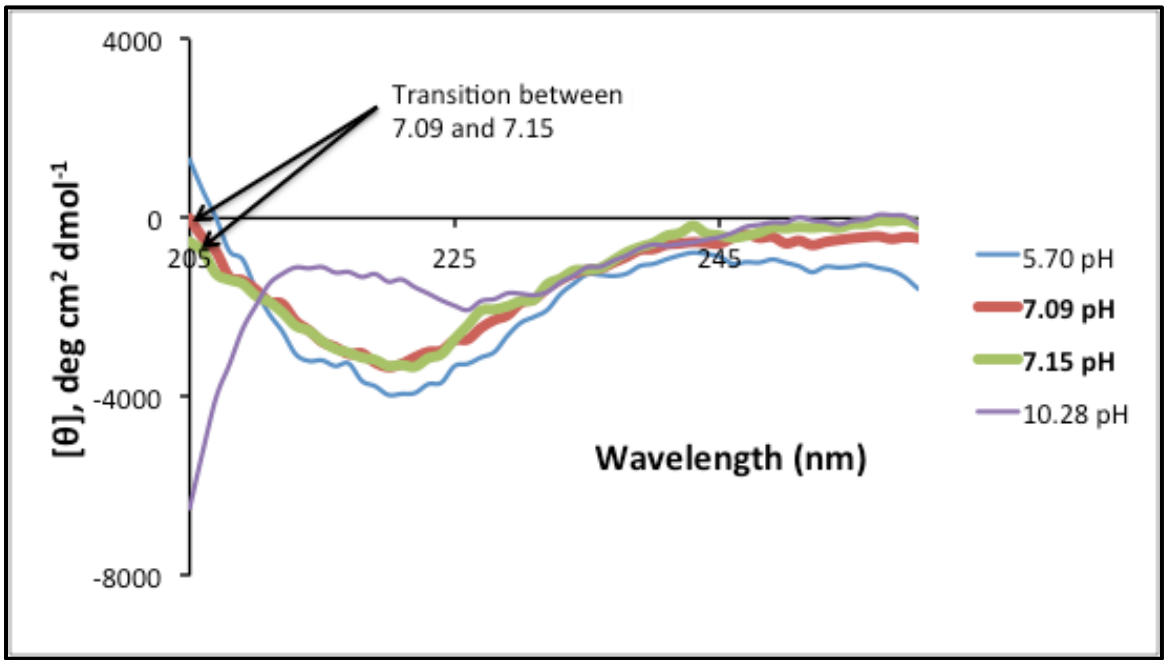

Figure 3.7: pH-dependent CD spectra of 10 µM palmitoyl-AIAAEEEEK(DO3A:Gd)-NH_2

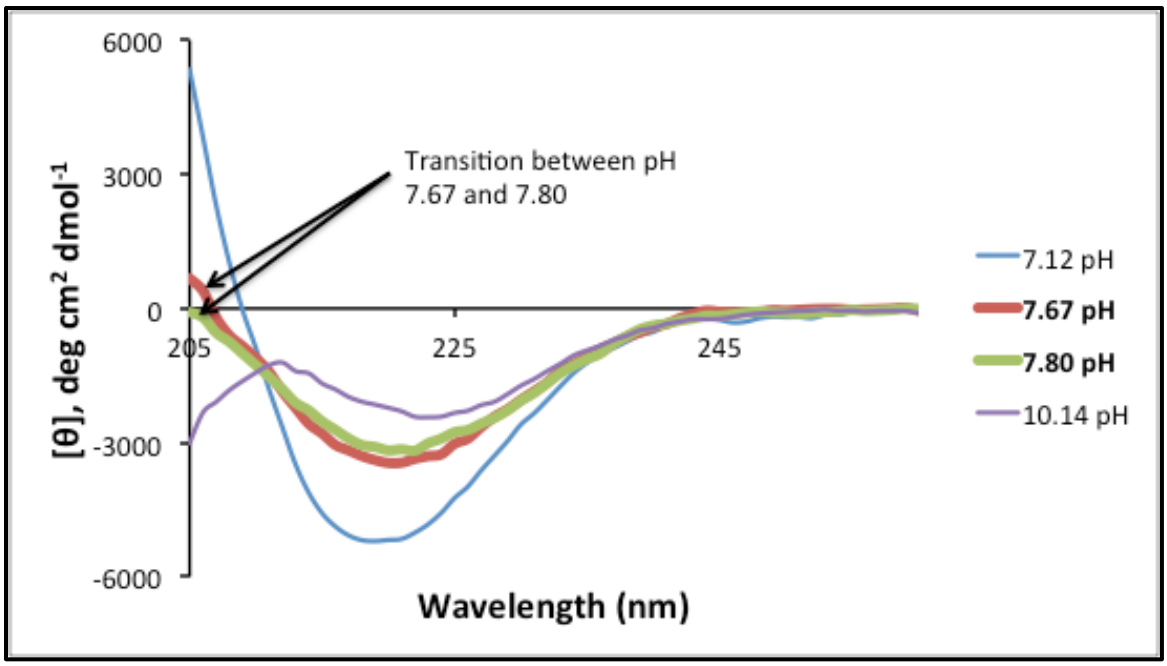

Figure 3.8: pH-dependent CD spectra of 25 µM palmitoyl-AIAAEEEEK(DO3A:Gd)-NH_2

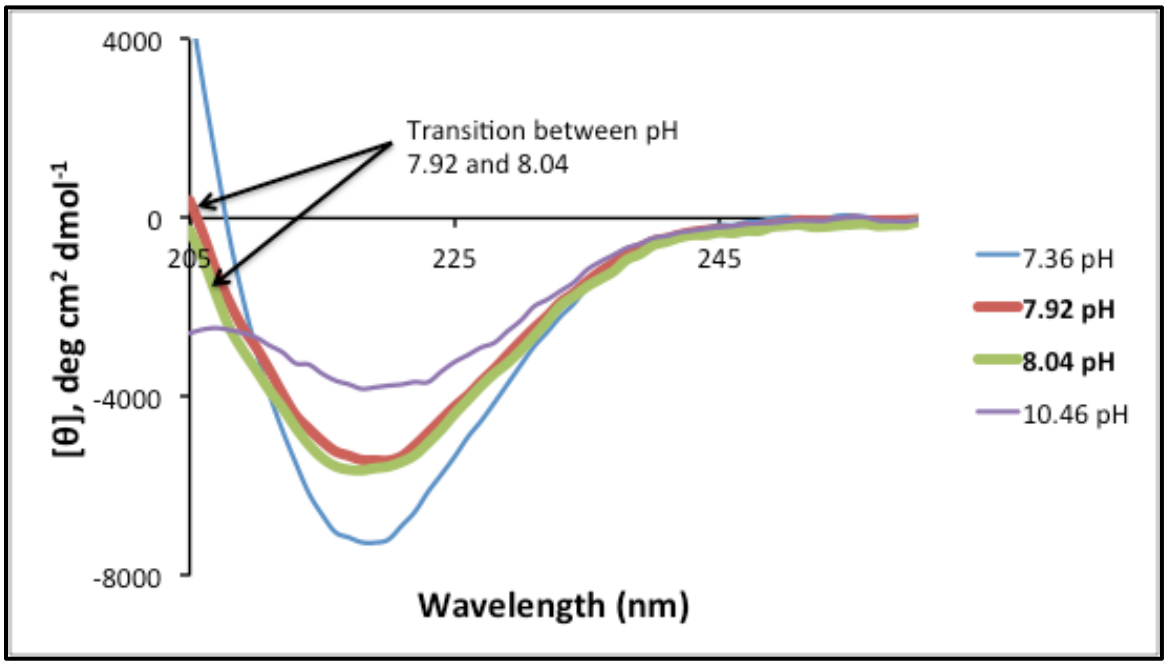

Figure 3.9: pH-dependent CD spectra of 50 µM palmitoyl-AIAAEEEEK(DO3A:Gd)-NH_2

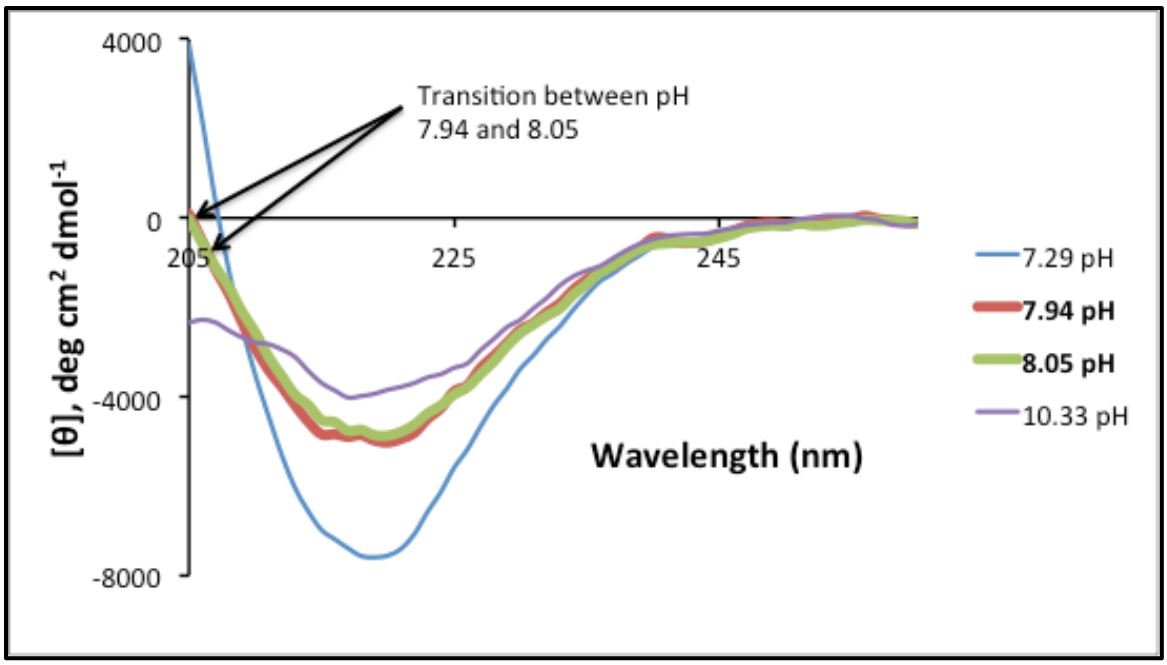

Figure 3.10: pH-dependent CD spectra of 150 µM palmitoyl-AIAAEEEEK(DO3A:Gd)-NH_2

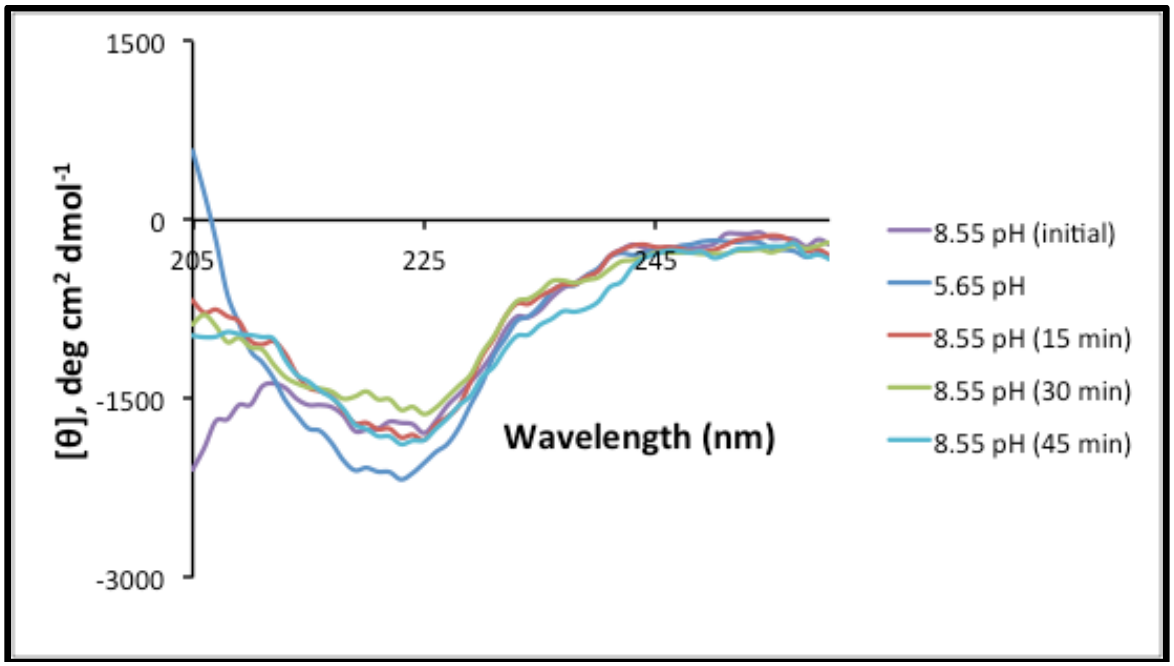

Figure 3.11: Reversibility of transition, 5 µM palmitoyl-AIAAEEEEK(DO3A:Gd)-NH_2

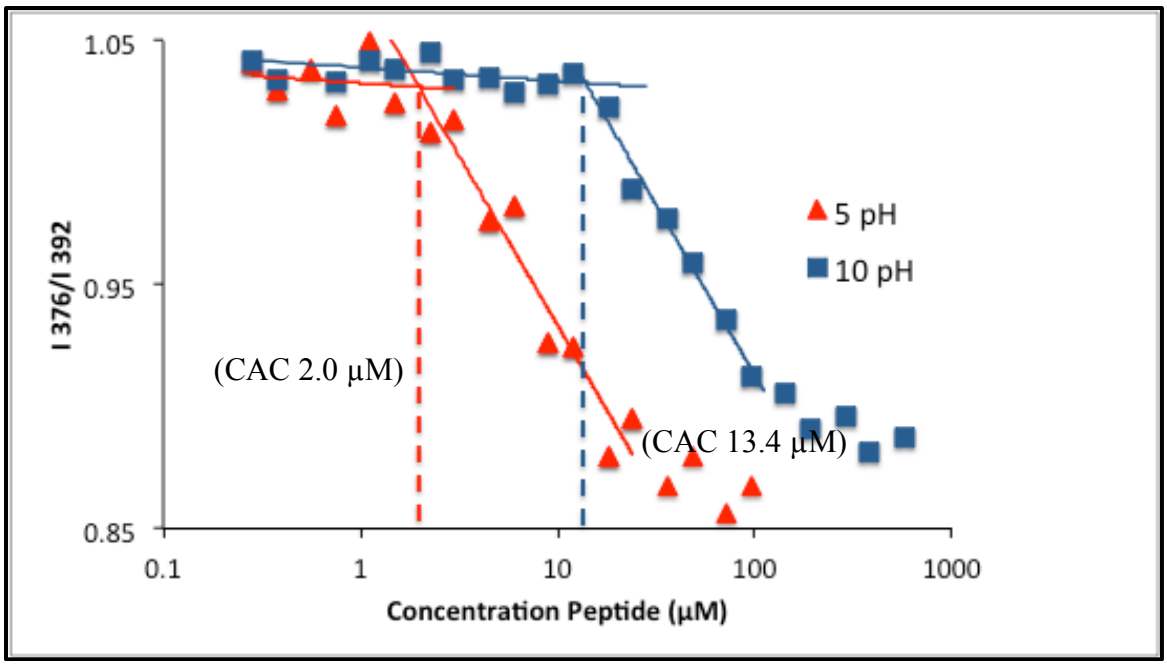

Figure 3.12: palmitoyl-AIAAEEEE-NH_2 pH-dependent CAC determination (pH 5 &10)

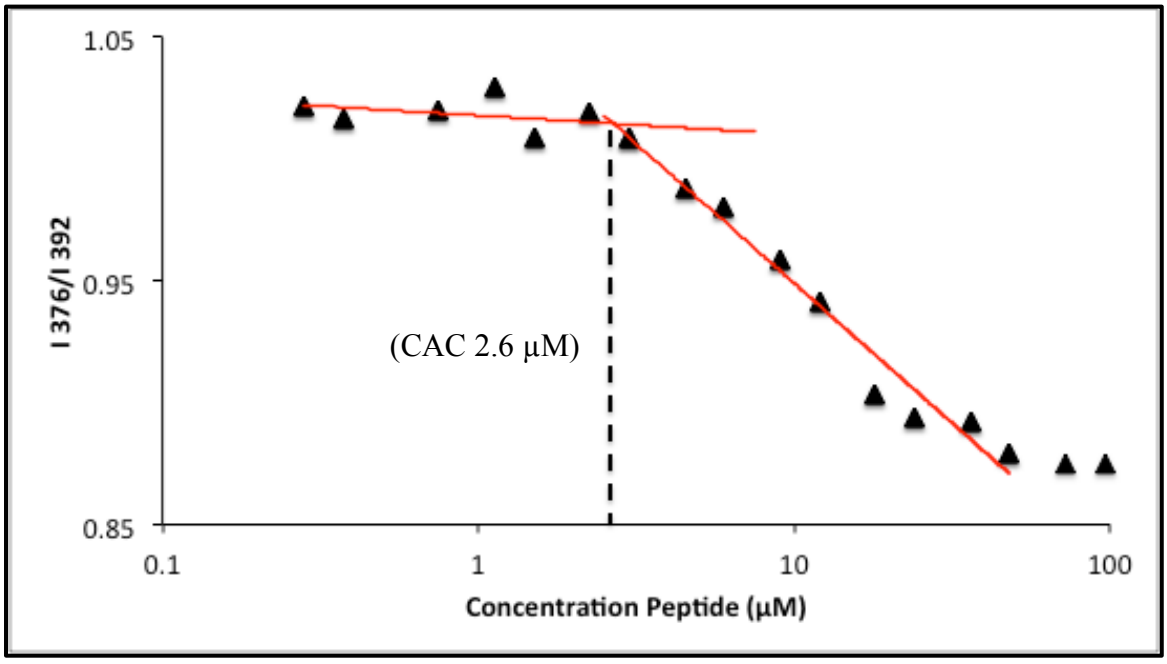

Figure 3.13: palmitoyl-AIAAEEEE-NH_2 CAC determination at pH 6

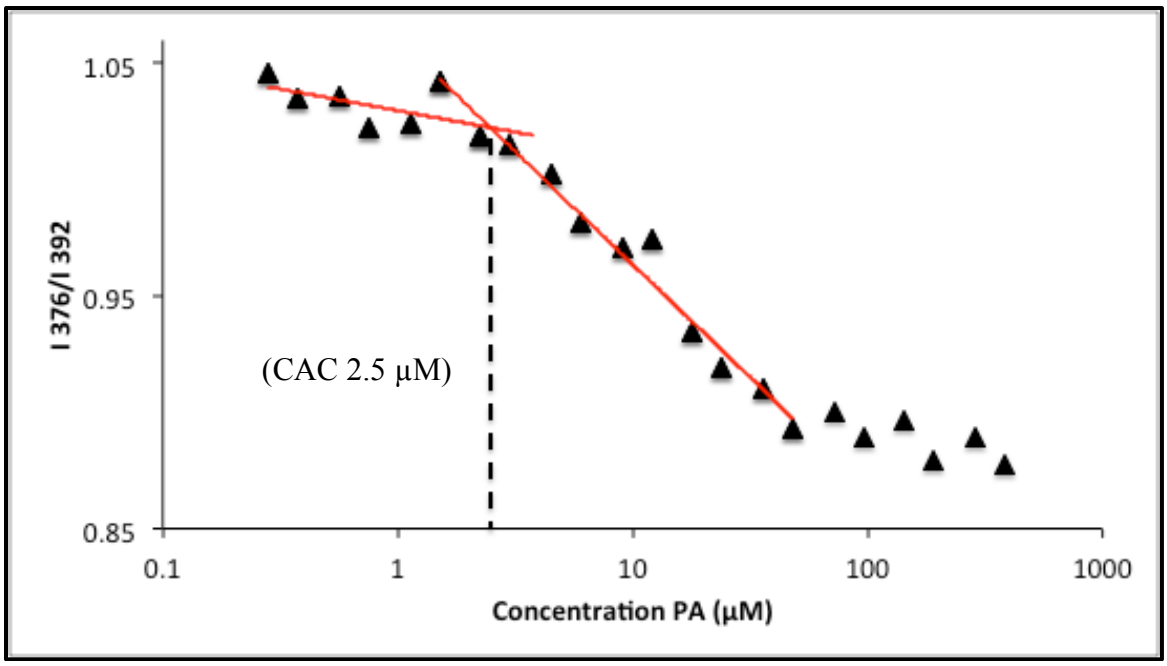

Figure 3.14: palmitoyl-AIAAEEEE-NH_2 CAC determination at pH 7

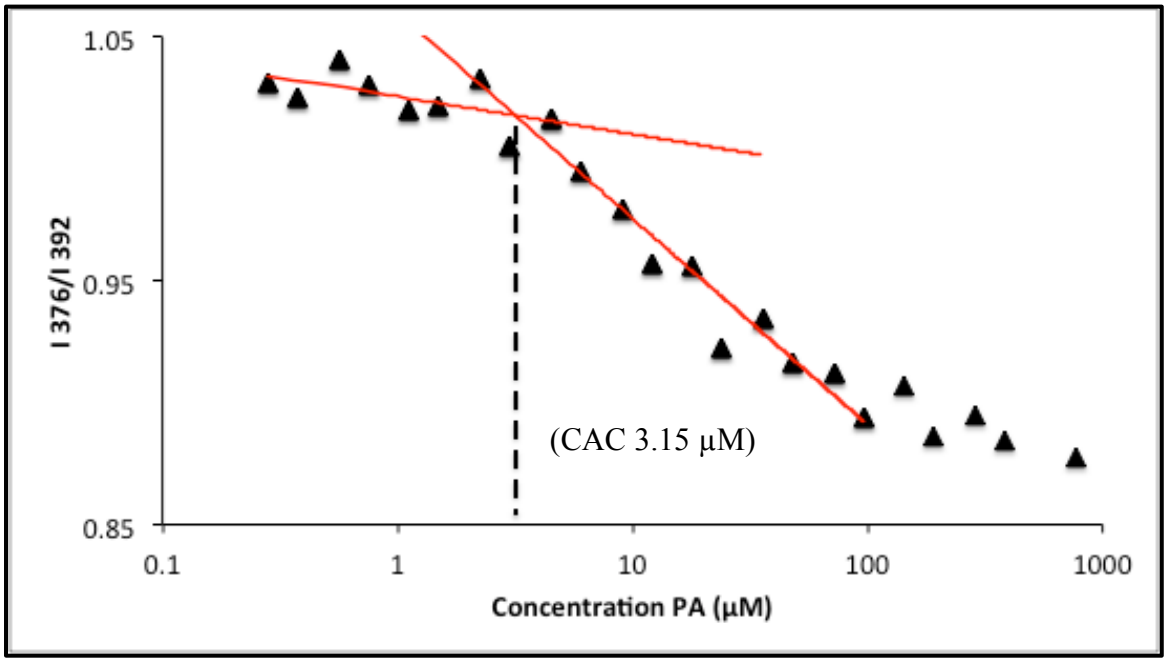

Figure 3.15: palmitoyl-AIAAEEEE-NH_2 CAC determination at pH 8

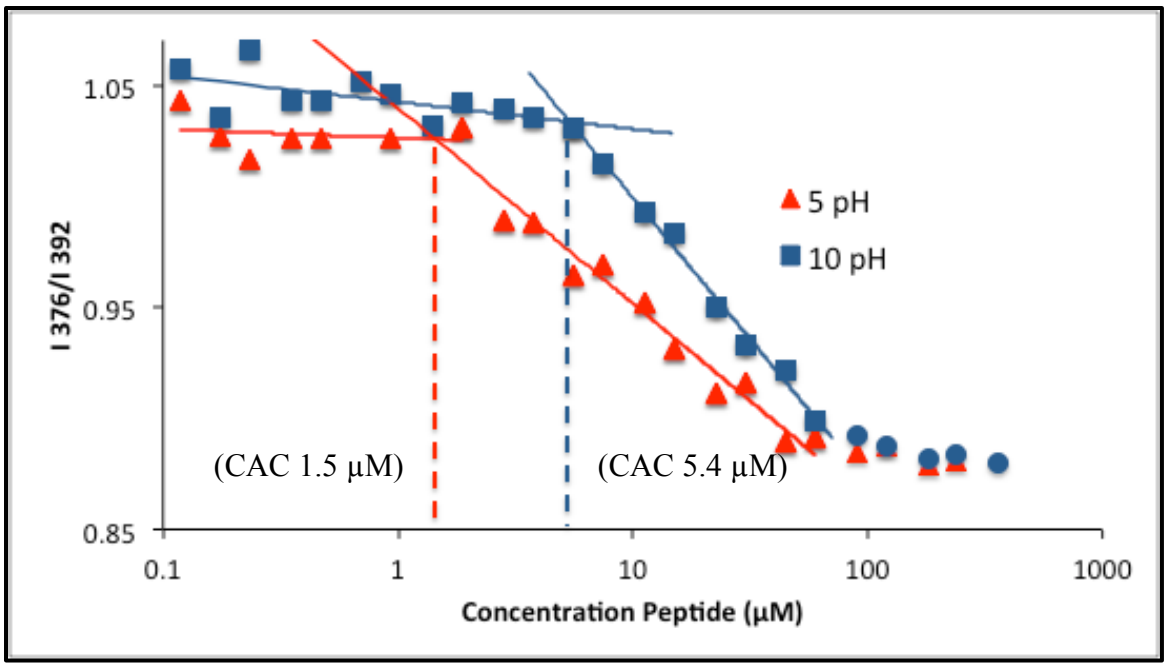

Figure 3.16: palmitoyl-AIAAEEEEK(DO3A:Gd)-NH_2 pH-dependent CAC determination (pH 5 &10)

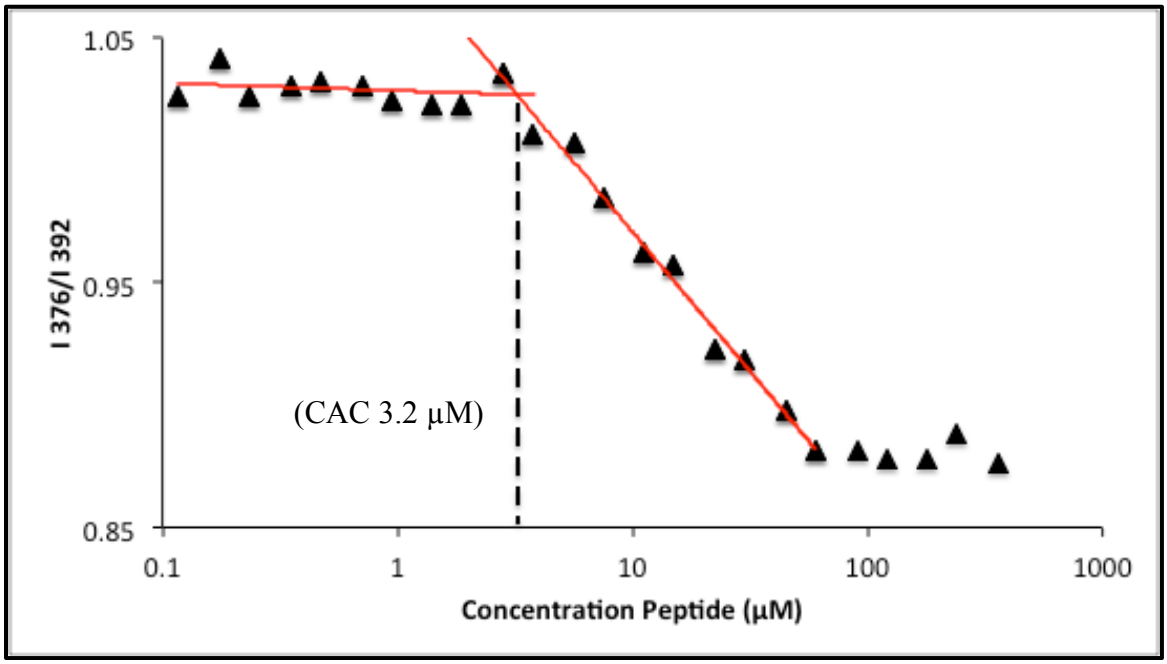

Figure 3.17: palmitoyl-AIAAEEEEK(DO3A:Gd)-NH_2 CAC determination at pH 6

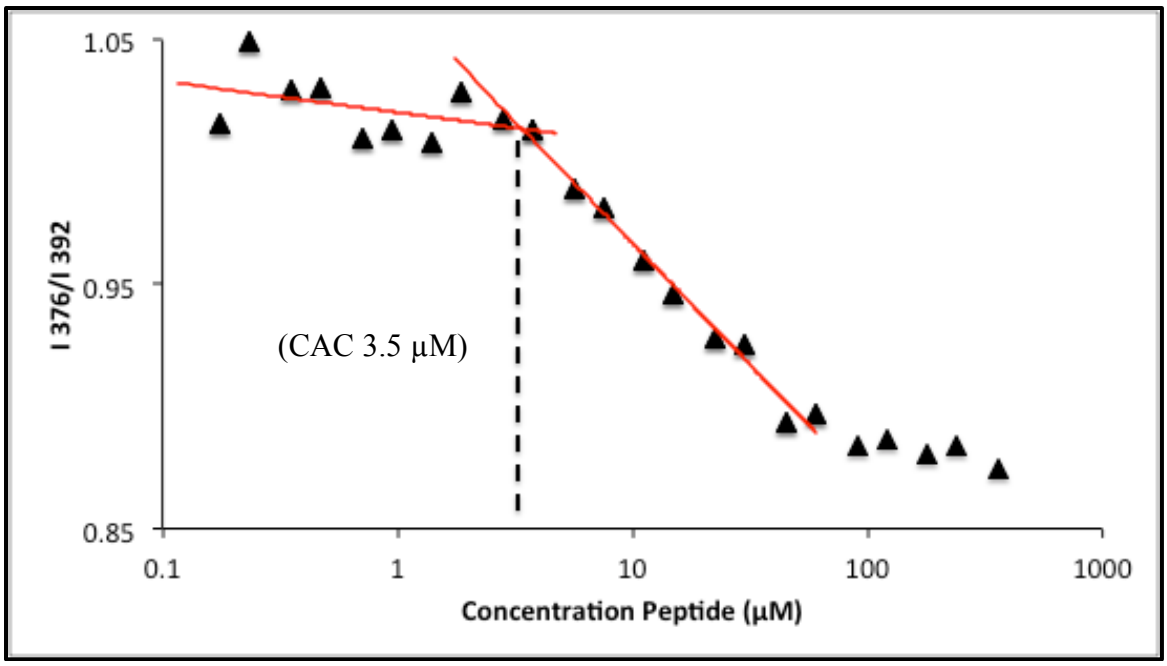

Figure 3.18: palmitoyl-AIAAEEEEK(DO3A:Gd)-NH_2 CAC determination at pH 7

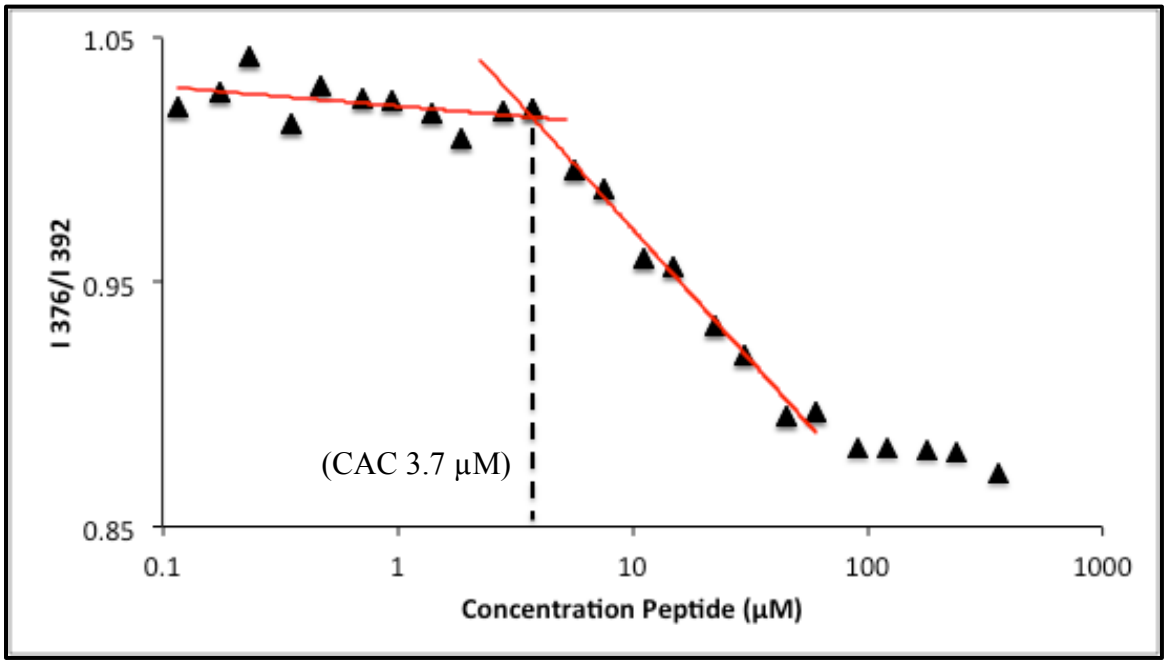

Figure 3.19: palmitoyl-AIAAEEEEK(DO3A:Gd)-NH_2 CAC determination at pH 8

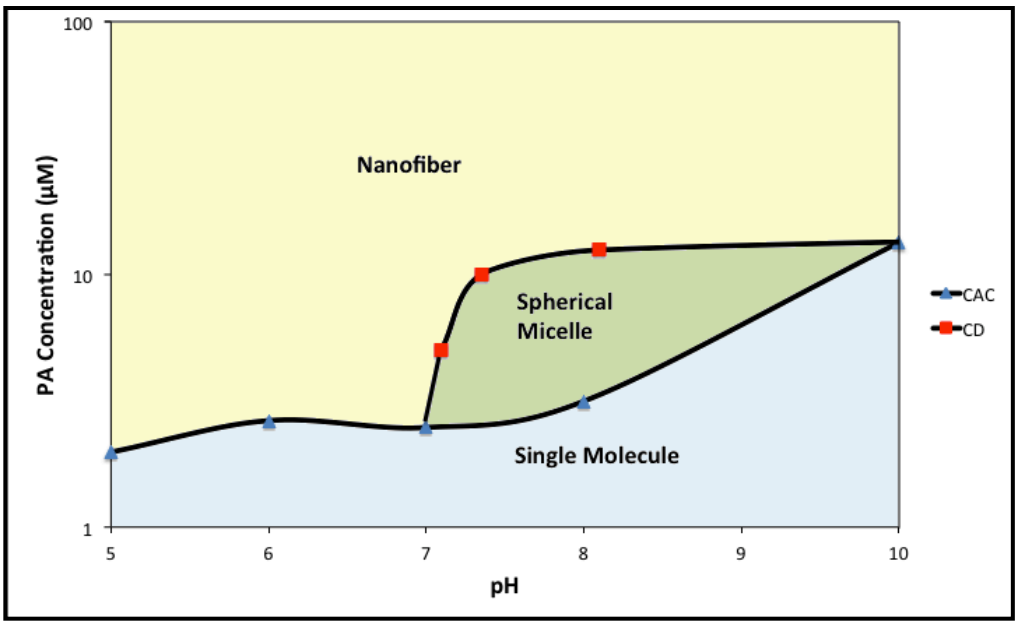

Figure 3.20: palmitoyl-AIAAEEEE-NH_2 phase diagram

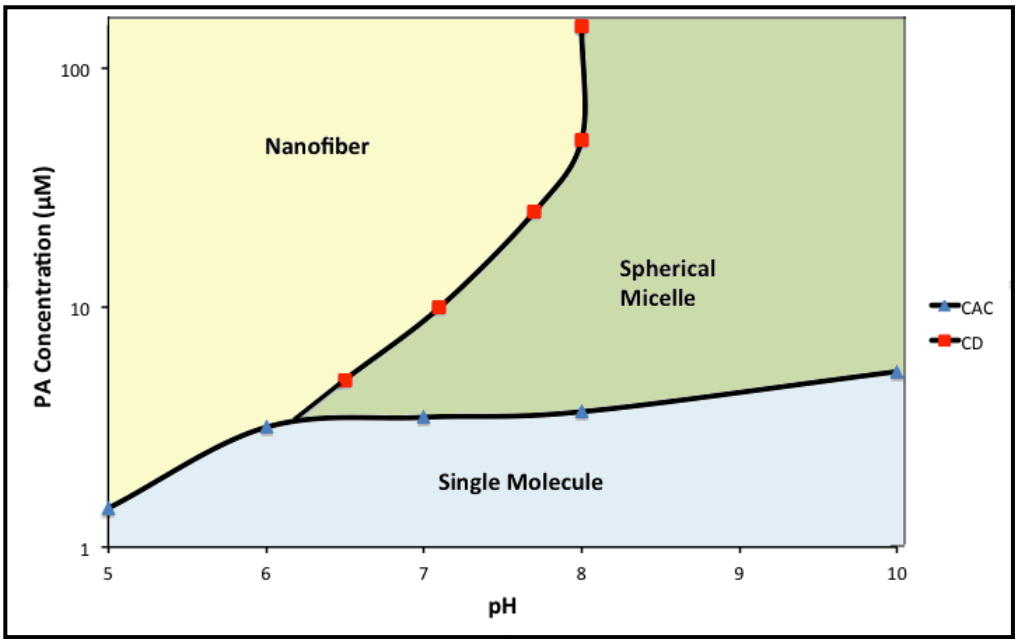

Figure 3.21: palmitoyl-AIAAEEEEK(DO3A:Gd)-NH2 phase diagram

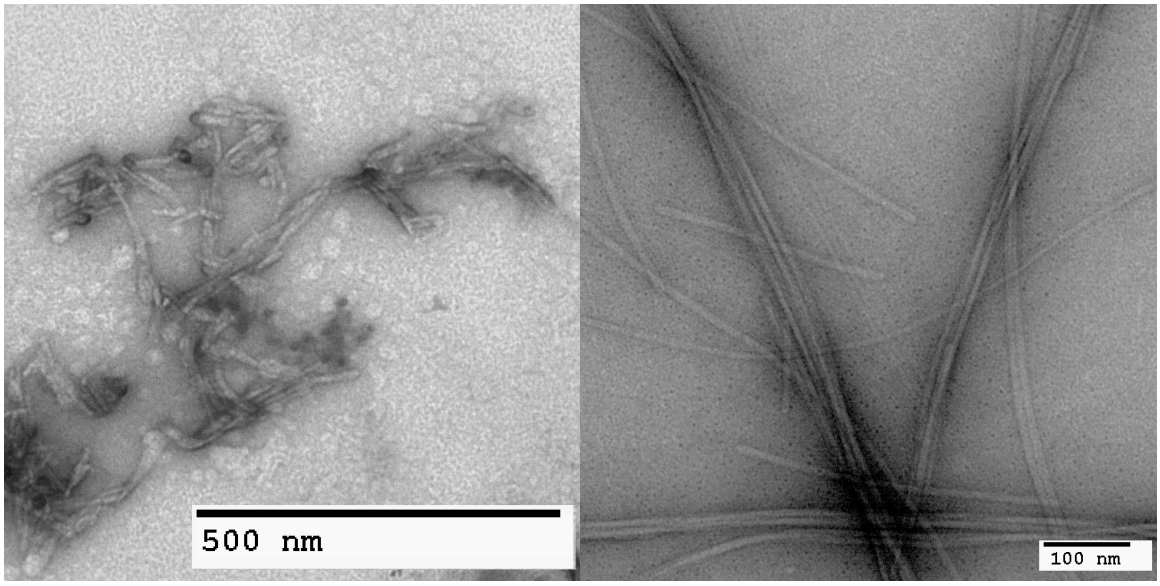

Figure 3.22: TEM images of 10 μM palmitoyl-AIAAEEEE-NH_2 at 5.5 pH (left) and 100 μM at 8.3 pH (right)

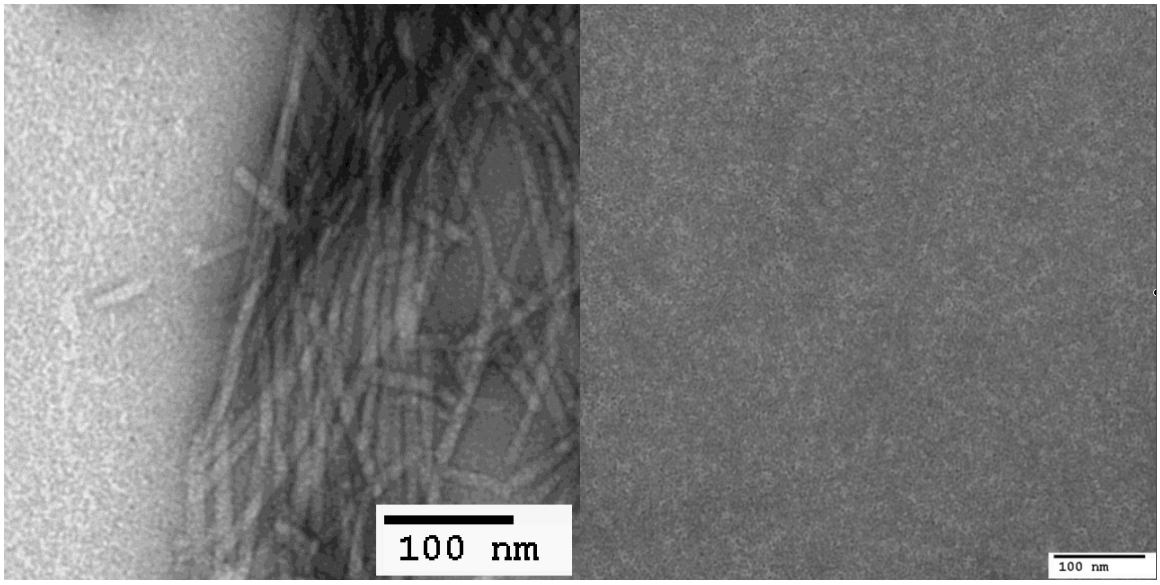

Figure 3.23: TEM images of 150 μM palmitoyl-AIAAEEEEK(DO3A Gd) at pH 6.6 (left) and 9.9 (right)

Chapter 4

Comparison of Isomerized Peptide Amphiphiles

By overlaying the phase diagrams of isomeric PAs lacking the DO3A imaging moiety (Figure 4.1) and the phase diagrams of isomeric PAs with the DO3A imaging moiety (Figure 4.2), the effects of sequence variation within the β sheet-forming region were analyzed. The creation of sequence variants in both cases resulted in lower CAC concentrations at nearly all pH values. Therefore, moving the Ile residue to the second position promotes single molecule aggregation.

By examining CD data in each phase diagram, it is evident that by moving Ile to the second beta sheet forming position, aggregation from spherical micelle to nanofiber is promoted at higher pH. This is most evident in the DO3A-containing molecules (Figure 4.2) due to their lower concentration dependence. For instance, at 10 μM palmitoyl-AIAAEEEEK(DO3A:Gd)-NH_2 transitions from sphere-to-nanofiber at pH 7.1. This transition pH is nearly 1.5 units higher than that for palmitoyl-IAAAEEEEK(DO3A:Gd)-NH_2 at the same concentration. Notably, palmitoyl-AIAAEEEEK(DO3A:Gd)-NH_2 shows a much higher concentration dependence for its transition than palmitoyl-IAAAEEEEK(DO3A:Gd)-NH_2. Between 10 and 500 μM, the pH for transition of palmitoyl-IAAAEEEEK(DO3A:Gd)-NH_2 lies in the range from 5.66 to 6.02 (less than 0.5 pH). Contrastingly, the transition for palmitoyl-AIAAEEEEK(DO3A:Gd)-NH_2 between 5 and 150 μM spans a range from 6.5 to 8.0 (pH 1.5). This concentration

dependence seems to decrease at high concentrations for palmitoyl-AIAAEEEEK(DO3A:Gd)-NH_2, since between 50 and 150 μM the transition remains constant at pH 8.0

Comparison of the CD data for non-DO3A-containing isomers is more difficult due to the high concentration dependence the sphere-to-nanofiber transition exhibits for both isomers. In general, palmitoyl-AIAAEEEE-NH_2 seems to favor the nanofiber morphology at higher pH values compared to palmitoyl-IAAAEEEE-NH_2. At 10 μM, palmitoyl-IAAAEEEE-NH_2 displays a sphere-to-nanofiber transition at pH 6.5, while its isomer shows a transition at pH 7.35 (a shift of nearly 0.9 pH unit). Additionally, palmitoyl-IAAAEEEE-NH_2 exhibits a solely nanofiber morphology above 20 μM concentration while its isomer is exclusively nanofibers at all concentrations above 15 μM.

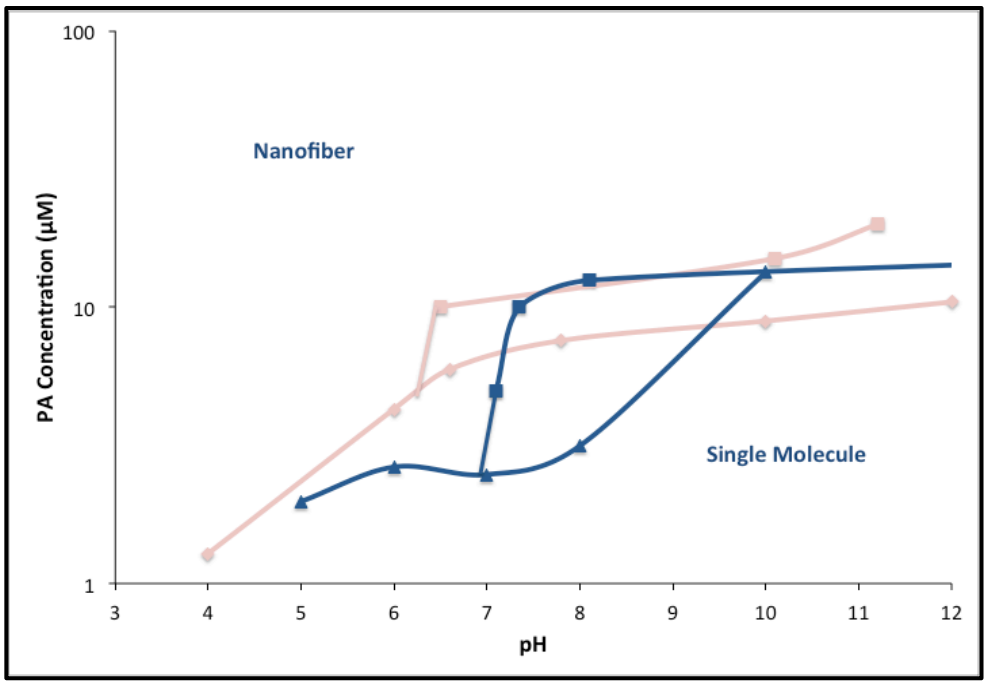

Figure 4.1: Superimposed phase diagrams of palmitoyl-AIAAEEEE-NH_2 (blue) and palmitoyl-IAAAEEEE-NH_2 (pink)

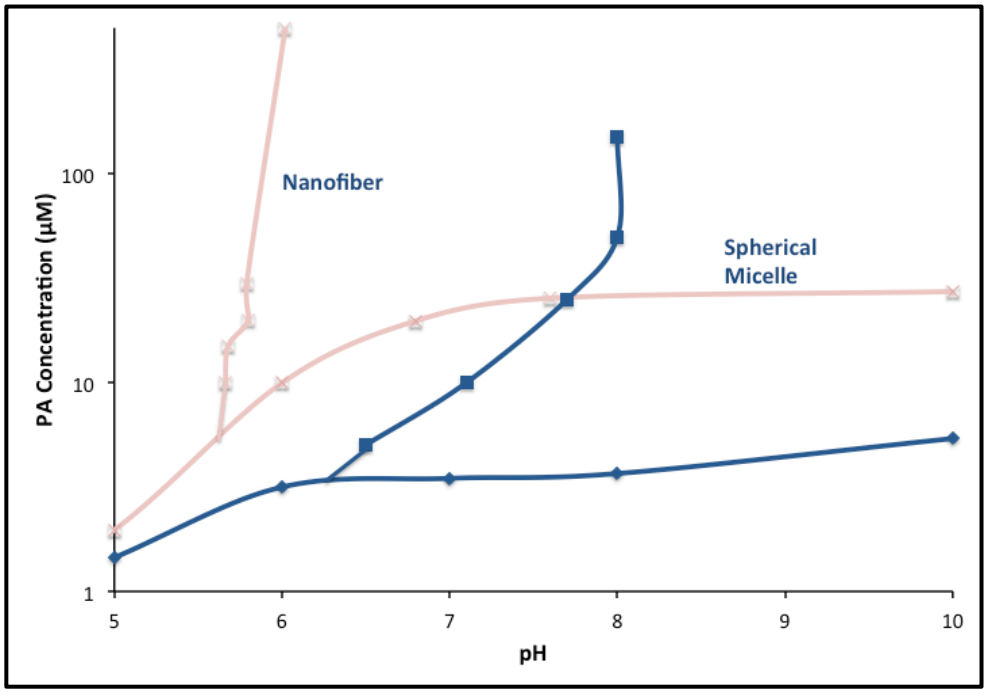

Figure 4.2: Superimposed phase diagrams of palmitoyl-AIAAEEEEK(DO3A:Gd)-NH_2 (blue) and palmitoyl-AIAAEEEEK(DO3A:Gd)-NH2 (pink)

Chapter 5

Conclusions and Future Directions

In exploring the effects of β sheet isomerization on pH-triggered PA self-assembly, creating a space of one amino acid between the β sheet-forming residue and the hydrophobic core enhances aggregation of single molecules into nanofibers or spheres (CAC) and of spherical micelles into longer nanofibers (CD). These trends held true regardless of whether a -K(DO3A:Gd)-NH_2 head group was included in the PA structure. For PAs lacking the MRI-active head group, shifting Ile to the second position causes the CAC to decrease by half or more. For PAs containing the MRI-active head group, the isomerization had an even great impact, decreasing CAC by as great as seven-fold. The transition from sphere-to-nanofiber of palmitoyl-AIAAEEEEK(DO3A:Gd)-NH_2 was observed to be more than 2 pH units higher than palmitoyl-IAAAEEEEK(DO3A:Gd)-NH_2. Self-assembly of palmitoyl-AIAAEEEE-NH_2 into nanofibers was also shifted to 1 pH unit higher than palmitoyl-IAAAEEEE-NH_2 at 10 μM. These shifts resulting from isomerization are more drastic than what was previously observed by adding or changing the identity of the first amino acid residue[17].

Recent coarse-grained (CG) molecular dynamics (MD) simulations on a similar PA system, palmitoyl-VVVAAAEEE-NH_2, suggest that hydrophobic residues positioned near the hydrophobic core of a micelle tend to associate with the hydrophobic core, collapsing inward (Figure 5.1). Additionally, calculations using this CG MD model of palmitoyl-VVVAAAEEE-NH_2 revealed that the highest degree of β-sheet character was

in amino acid residues 2-5 and that the percent β character in residue 1 was less than 10% (Figure 5.1)[23]. Therefore the drastic shift in transition pH between the isomeric PA systems studied here is attributed to the fact that, when positioned next to the palmitoyl acid tail, the β sheet forming residues like Ile or Val more readily associate with the hydrophobic tail, destabilizing the β sheet. As a hydrophobic residue, the positioning of Ile near the palmitoyl tail causes the residue to either participate in the hydrophobic collapse near the micelle's core or to facilitate hydrogen bonding with neighboring PAs, assisting in the creation β sheet secondary structure. Hydrophobic collapse precludes Ile from participating in hydrogen bonding, and vice versa. Additionally, this collapse interrupts the formation of hydrogen bonds N-terminal to the interruption (Figure 5.2). By creating distance between Ile and the hydrophobic core (via isomerization), hydrophobic collapse of the Ile becomes less favorable. Instead, the Ile hydrogen bonds with nearby residues of neighboring molecules (Figure 5.3). This results in the PA more readily assuming a nanofiber morphology.

Importantly, the sphere-to-nanofiber transition of palmitoyl-AIAAEEEEK(DO3A:Gd)-NH_2 between 5 and 20 μM falls well within the desired range for tumor targeting (pH 6.6-7.4). For the most part, this aggregation falls at or above the detectable limit for MRI contrast agents. Therefore, this PA seems to be well suited for future *in vivo* assays.

Our increase in understanding of the structure property relationships with the creation of just two pairs of isomers merit further investigation of other isomeric relationships. First, the creation of more isomers from the same parent molecules (β

sheet sequences of –AAIA- and –AAAI-) should further confirm the role of hydrophobic amino acid isomerization on dynamic PA self-assembly. Additionally, creating pairs or quadruplets of isomers containing a β sheet-forming amino acids other than Ile would verify that these results may be generalized to all PAs within this dynamic pH-trigger self-assembly class. Since Ile has the highest β sheet propensity of any amino acid, an amino acid of particularly low a β sheet-forming propensity, such as tyrosine, would be interesting to study. Specifically, study of palmitoyl-YAAAEEEEK(DO3A:Gd)-NH_2 and its isomers may yield valuable insight into the factors affecting PA self-assembly. In summary, varying the amino acid sequence provides an alternate mechanism for drastically changing the dynamic self-assembly behavior of PAs. This method will be used in the future for more intelligent programming of PA self-assembly.

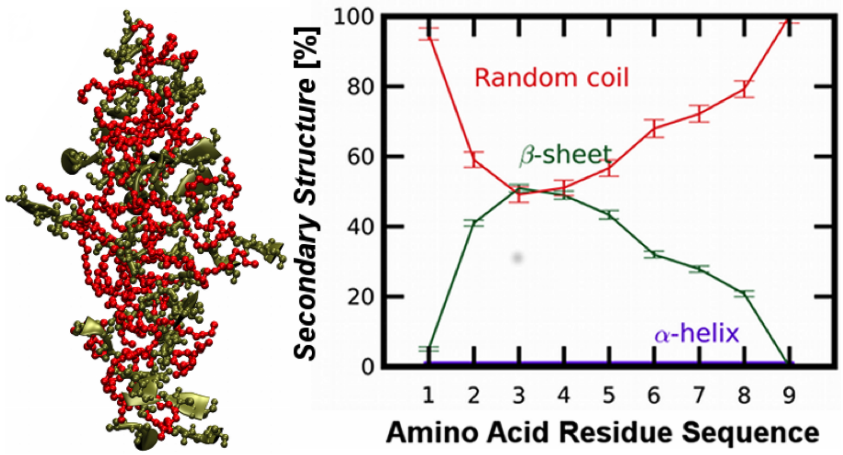

Figure 5.1: Hydrophobic core of palmitoyl-VVVAAAEEE-NH_2 comprised of alkyl tails (red) and valine residues (green) (left)[23] and percentages of secondary structures for each amino acid residue in palmitoyl-VVVAAAEEE-NH_2 (right)[23]

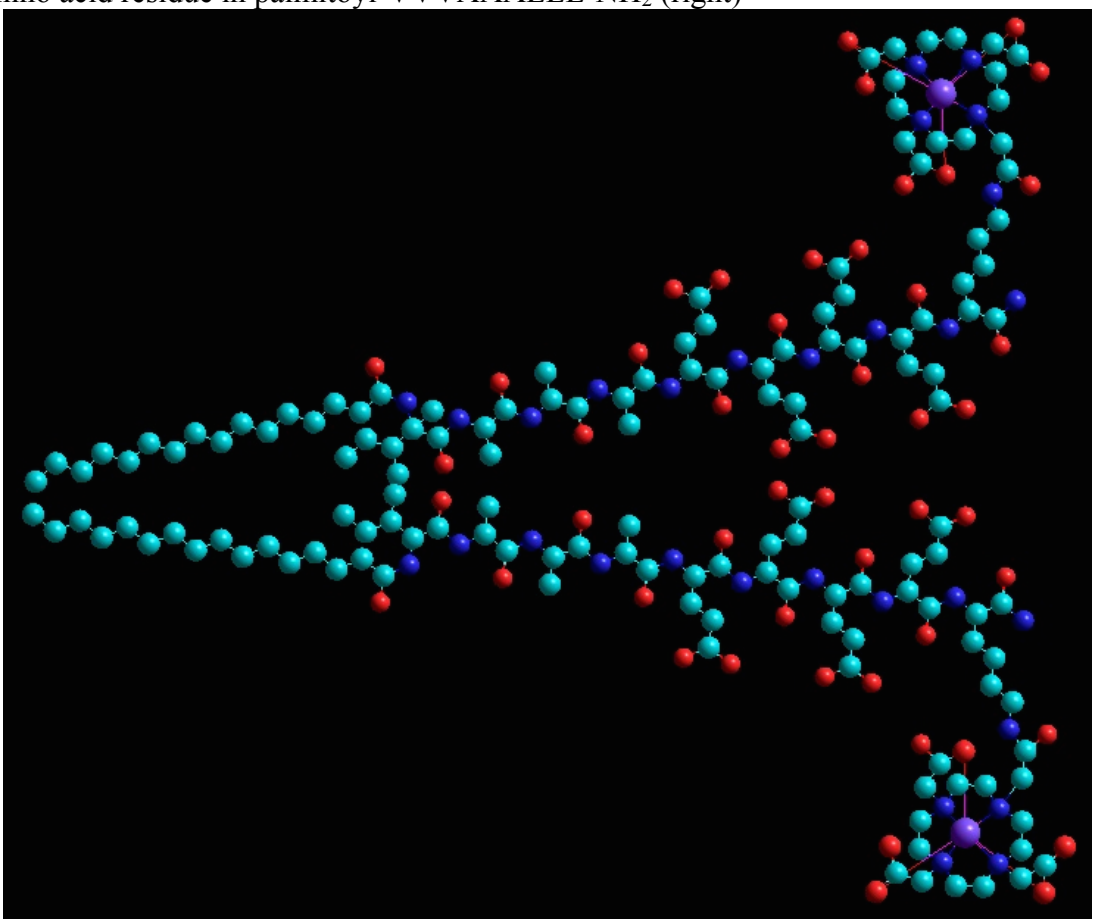

Figure 5.2: Schematic representation of palmitoyl-IAAAEEEEK(DO3A:Gd)-NH_2 highlighting Ile association with the hydrophobic tail, thus destabilizing β-sheet formation.

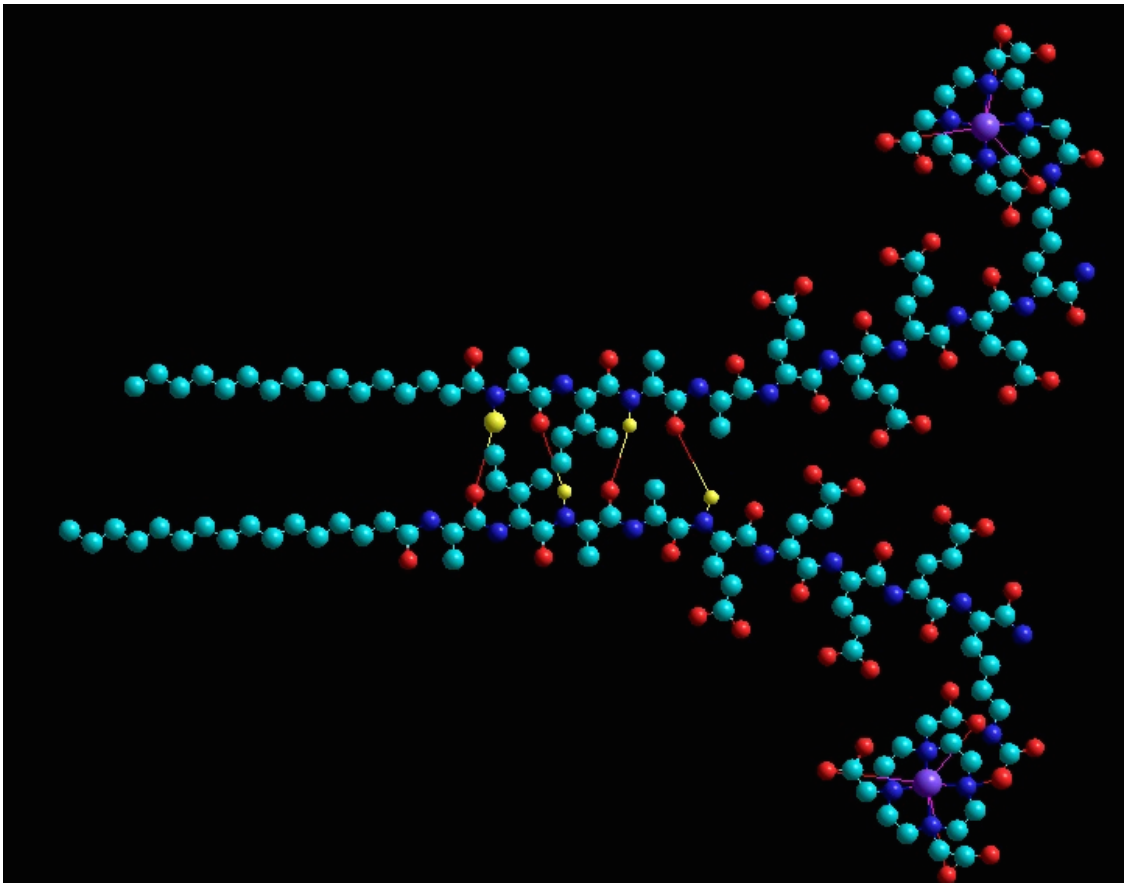

Figure 5.3: Schematic representation of palmitoyl-AIAAEEEEK(DO3A:Gd)-NH_2 more strongly participating in hydrogen-bonding.

References

(1) "Cancer." World Health Organization. Web. 2012.

(2) "Cancer of the Breast." Surveillance Epidemiology and End Results. Web. 2011.

(3) Cho, S.; et al. *J Breast Cancer* **2012**, 15(3): 265–272.

(4) Kolata, Gina. "A New Treatment's Tantalizing Promise Brings Heartbreaking Ups and Downs." *The New York Times*. 8 July **2012**.

(5) Gerlinger, M.; et al. *N Engl J Med* **2012**, 336:883-392.

(6) Geng, Y.; Dalhaimer, P.; Cai, S.; Tsai, R.; Tewari, M.; Minko, T.;Discher, D. E. *Nat. Nanotech* **2007**, 2, 249.

(7) Petros, R. A.;DeSimone, J. M. *Nat. Rev. Drug Discov*. **2010**, 9, 615.

(8) Yoo, J.-W.;Irvine, D. J.; Discher, D. E.; Mitragotri, S. *Nat. Rev. Drug Discov*. **2011**,10, 521.

(9) Popovic, Z.; Liu, W.; Chauhan, V. P.; Lee, J.; Wong, C.;Greytak, A. B.; Insin, N.; Nocera, D. G.; Fukumura, D.; Jain, R. K.;Bawendi, M. G. Angew. *Chem Int Ed*. **2010**, 49, 8649.

(10) Geng, Y.; Dalhaimer, P.; Cai, S.' Tsai, R.; Tewari, M.; Minko, T.; Discher, D. E. *Nat Nanotech* **2007**, 2, 249.

(11) Caron Y. P; Song G.; Kumar P.; Rawal S.; Zamboni W. C. *Clin Pharmacol Ther.* **2012**, 5, 802-812.

(12) Jain R. K.; Stylianopoulos T. *Nat Rev Clin Oncol*. **2010**, 7, 653-664.

(13) Torchilin, V. P. *Pharm Res*. **2007**, 24, 1.

(14) Gatenby, R. A.; Gillies, R. J. *Nat Rev Cancer.* **2004**, 4, 891.

(15) Cui, H.; Webber, M. J.; Stupp, S. I. *Biopolymers*. **2010**, 94(1):1-18.

(16) Wedeking, P.; Shukla, R.; Kouch, Y. T.; Nunn, A. D.; Tweedle, M. F. *Magnetic Resonance Imaging* **1999**, *17*, 569.

(17) Ghosh A, Haverick M, Stump K, Yang X, Tweedle MF, Goldberger JE. *J Am Chem Soc.* **2012**, 134(8): 3647-3650.

(18) Han S, Cao S, Wang Y, Wang J, Xia D, Xu H, Zhao X, Lu JR. *Chemistry* **2011**; 17(46): 13095-13102.

(19) Zhao Y, Wang J, Deng L, Zhou P, Wang S, Wang Y, Xu H, Lu JR. *Langmuir* **2013**, 29(44): 13457-13464.

(20) King, D. S.; Fields, C. G.; Fields, G. B. *Int J Pept Protein Res.***1990**, 36, 255.

(21) Aguiar, J.; Carpena, P.; Molina-Bolivar, J. A.; Ruiz, C. C. J. *Colloid Interface Sci*. **2003**, 258, 116.

(22) Greenfield, N. J. *Nat. Protocols* **2007**, 1, 2876.

(23) Fu I. W.; Markegard C. B.; Chu B. K.; Nguyen H. D. *Adv Healthcare Mater*. **2013**, 10.